International Journal of Optics

The Future of Opto-Electronics: Device Architecture, Novel Materials, and Applications

Lead Guest Editor: Preeti Singh
Guest Editors: Charu Madhu, Nidhi Garg, Pardeep Kaur, and Gaurav Madhu

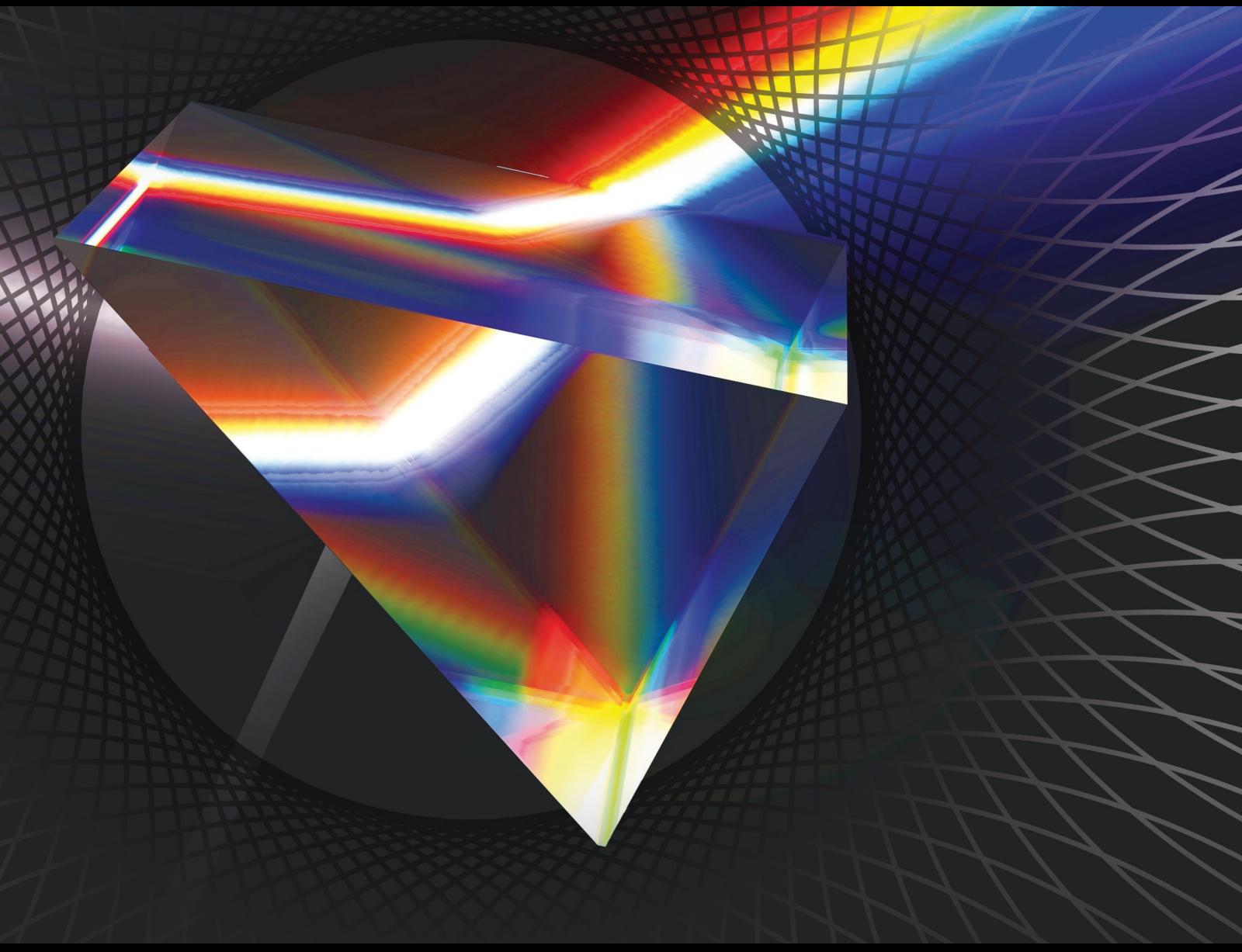

The Future of Opto-Electronics: Device Architecture, Novel Materials, and Applications

International Journal of Optics

The Future of Opto-Electronics: Device Architecture, Novel Materials, and Applications

Lead Guest Editor: Preeti Singh
Guest Editors: Charu Madhu, Nidhi Garg, Pardeep Kaur, and Gaurav Madhu

Contents

Hindawi
International Journal of Optics
Volume 2021, Article ID 9950202, 20 pages
https://doi.org/10.1155/2021/9950202

Review Article

Dielectric Properties of ZnO-Based Nanocomposites and Their Potential Applications

Daljeet Kaur,[1,2] **Amardeep Bharti**,[3] **Tripti Sharma**,[2] **and Charu Madhu**[1]

[1]*University Institute of Engineering and Technology, Panjab University, Chandigarh 160014, India*
[2]*Chandigarh University, Mohali, Punjab 140413, India*
[3]*Elettra Sincrotrone Trieste, S.C.p.A., Basovizza 34149, Italy*

Correspondence should be addressed to Amardeep Bharti; abharti_phy@yahoo.com and Charu Madhu; charunarula81@gmail.com

Received 11 March 2021; Accepted 14 July 2021; Published 22 July 2021

Academic Editor: Wonho Jhe

Energy storage devices constitute one of the research areas in recent years. Capacitors are commonly used for the storage of electrical energy. The current research is focusing on not only the improvement in energy density but also the materials which are environment friendly. Polymer composites are known to be technically essential materials owing to their wide range of applications. Enormous research has been devoted to zinc oxide- (ZnO-) based polymer nanocomposites, due to their extraordinary dielectric properties. This review article presents a detailed study of the dielectric properties of ZnO-based nanocomposites. The dielectric constant study includes the effect of transition metals and rare earth metals as a dopant in ZnO. This review gives an insight into the mechanism responsible for the variation of dielectric constant in ZnO nanocomposites due to various factors like size of nanoparticles, thickness of the thin film, operating frequency, doping concentration, and atomic number. The observations have been summarized to convey the mechanism and structural changes involved in the ZnO nanocomposites to the researchers. The deployment of biodegradable nanocomposite materials is expected to open an innovative way for their outstanding electronic applications as storage materials.

1. Introduction

The dielectric properties of material define its characteristic role in electronics. To study the dielectric properties of any material, dielectric constant (k) is a crucial factor that determines the charge storage capability of the material [1]. High-k materials are used as gate dielectrics in MOS transistors, memory cells, capacitors, supercapacitors [2, 3], and so forth, whereas low-k materials find their applications in electrical insulation and high-speed integrated circuits [4]. The semiconductor industry is greatly influenced by dielectric materials and emerges out as a revolutionary stream of microelectronics [5]. Metal oxide dielectric materials are considered to be a key element for diverse thin-film electronic systems owing to their superior dielectric and mechanical properties [6]. Titanium dioxide (TiO_2) in rutile form exhibits a high dielectric constant and can be used as a filler in hybrid (i.e., organic-inorganic) composites for application in modern electronics [7, 8]. Tin dioxide (SnO_2) is an n-type semiconductor possessing a wide direct bandgap of 3.37 eV at room temperature [9]. Due to low electrical resistivity, high chemical, mechanical, and thermal stability [10], it is very useful for applications in spintronics [11], lithium-ion batteries (LIBs), and supercapacitors [12, 13]. Due to its high dielectric constant [14], SnO_2 can be used for applications in thin-film electrodes, sensors, batteries, and solar cells [15].

ZnO is a semiconductor of groups II-VI. It is actively used due to its very attractive properties and nontoxic nature. Among metal oxides, nanostructured zinc oxide (ZnO) exhibits exceptional electronic, optical, and electrochemical properties. In addition to this, the wide bandgap (3.37 eV) and massive exciton binding energy (60 meV) permit the material to operate at much higher voltage, frequency, and

temperature than conventional semiconductors [16]. Moreover, ZnO-based composites have shown up potential applications in the field of industrial electronic devices like transducers, electrochemical sensors, solar cells, supercapacitors, and lithium-ion batteries [17–19]. ZnO is the most widely used inorganic compound because of its unique electronic, physical, and chemical properties [20]. This review article deals with the fundamental aspects behind the dielectrics along with the effective role of particle size and metal doping in ZnO to study its dielectric behaviour. Furthermore, the relative effect of transition metal and rare-earth-metal are also discussed in detail towards the dielectric origin in ZnO. Lastly, ZnO doped biodegradable polymer nanocomposites and their applications have been discussed thoroughly in this study.

2. Dielectric Materials

Dielectric materials are insulating materials. However, dielectric materials have some additional properties as compared to insulators. As they do not allow the flow of charge through them, they permit exerting electrostatic field and hence storing charge [21]. The thin films made up of dielectric materials extend enormous applications in the electronic industry like barrier layers, gate oxide, varactor dielectrics, and electrical isolation between conductive regions [22]. Numerous transition metal oxides demonstrate colossal dielectric constant and therefore have enormous potential for applications in modern microelectronics for the development of new capacitors for energy storage [23]. Lunkenheimer et al. observed a larger dielectric constant in various transition metal oxide materials, for example, $CaCu_3Ti_4O_{12}$ has a k value of 17000 and La_2SrNiO_4 has a k value of 10000 for their application in capacitive circuits [23]. Meher et al. suggested that Sr_2TiMnO_6 can be used as dielectric material in capacitors, due to its large dielectric constant of the order of 10^5 [24]. The value of k is larger due to the high degree of polarization.

2.1. Polarization. When an atom is subjected to an electric field, it gives rise to the formation of a dipole [25]. If the dielectric material is subjected to an alternating field by placing it between two conducting plates acting as electrodes, it gives rise to the formation of a capacitor [26, 27] as shown in Figure 1. According to the equation of the capacitor,

$$C = \frac{(\varepsilon_0 \varepsilon_r A)}{d}. \quad (1)$$

Capacitance (C) depends upon four factors: area of the electrodes A, spacing between the electrodes d, permittivity of free space $\varepsilon_0 = 8.854 \times 10^{-14}$ F/cm, and relative permittivity or dielectric constant of the material ε_r.

All the dipoles within the dielectric material get aligned in the same direction as those of the applied electric field. The alignment of dipoles gives rise to an induced electric field which is in a reverse direction to the applied electric field

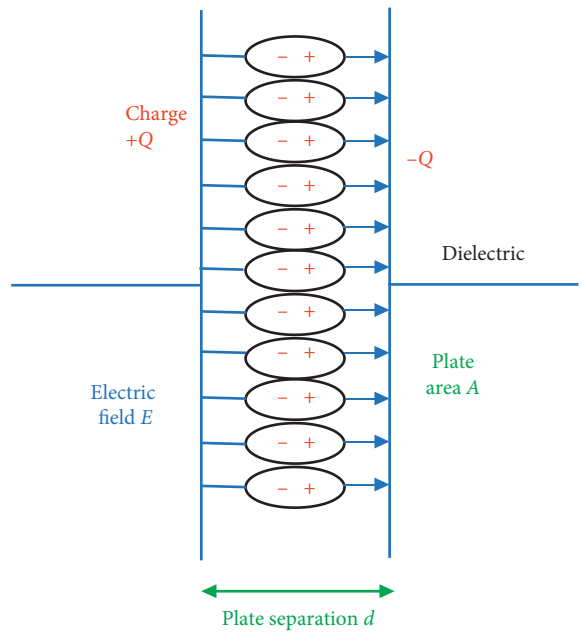

Figure 1: Structure of the dielectric capacitor.

[28, 29]. This process of alignment of dipoles is called polarization, due to which the material can store charge in it [30].

2.2. Source of Polarization. There are several aspects that give rise to polarization in the materials. Polarization is responsible for the relative permittivity of a material, subjected to an electric field [31]. It is originated from four different roots, namely, electronic, ionic, orientation, and interfacial polarization. Polarization is a frequency-dependent phenomenon [25, 32] as shown in Figure 2.

In a material, there may be single or multiple polarization sources active at a time. In a material having high relative permittivity, a greater number of sources or all these sources are active [31]. On the other hand, a few will be active in a material having low relative permittivity. In ZnO, all the four types of polarizations exist but the active one is dependent on the frequency of operation [33–37] The origin of high k in a material at low frequencies is the presence of all four sources of polarization, and it starts decreasing with the increase in frequency since dipoles in the material cannot follow the high frequency of applied field [38]. The value of k in a material increases with the increase in temperature which is attributed to the fact that a greater number of frozen dipoles are liberated due to thermal energy [39].

2.3. Dielectric Constant and Dielectric Loss. The ratio of absolute permittivity (ε) of the material and permittivity of free space (ε_0) is called relative permittivity (ε_r) or dielectric constant (k), which is represented as follows:

$$\varepsilon_r = \frac{\varepsilon}{\varepsilon_0}. \quad (2)$$

When a thick film of dielectric material is subjected to AC voltage, depending upon ε_r of the material, it permits or

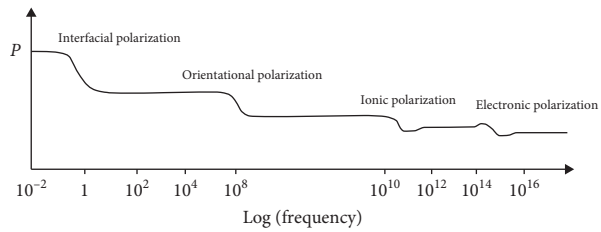

Figure 2: Frequency dependence of different dielectric polarizations.

allows the electric lines of force to get absorbed in it and gives rise to electric charge storage phenomena. The electric energy that does not get absorbed in the material and is dissipated in the form of heat is called dielectric loss. The complex permittivity of a material, which is subjected to an alternating field, is defined by the Debye expression [40–42]:

$$\varepsilon^{*}(\omega) = \varepsilon_{\infty} + \left(\frac{\varepsilon_s - \varepsilon_{\infty}}{1 + J\omega\tau}\right), \tag{3}$$

where ε_{∞} = dielectric constant at high frequency, ε_s = dielectric constant at low frequency, $\omega = 2\pi f$, τ = relaxation time, and $\varepsilon^{*}(\omega)$ is complex permittivity and is given by

$$\varepsilon^{*} = \varepsilon' - J\varepsilon'', \tag{4}$$

where ε' = real part of permittivity and is given by

$$\varepsilon' = \varepsilon_{\infty} + \left(\frac{\varepsilon_s - \varepsilon_{\infty}}{1 + \omega^2\tau^2}\right), \tag{5}$$

which is also called the real part of the complex dielectric constant (k). ε'' = imaginary part of permittivity and is given by

$$\varepsilon'' = \left(\frac{(\varepsilon_s - \varepsilon_{\infty})\omega\tau}{1 + \omega^2\tau^2}\right), \tag{6}$$

which is also called the imaginary part of the complex dielectric constant (k). ε' and ε'' both are frequency-dependent.

The dielectric loss factor is given by

$$\tan\delta = \frac{\varepsilon''}{\varepsilon'}. \tag{8}$$

Metal oxides possess a high dielectric constant along with low dielectric loss, thus having huge potential to be used in microelectronics industry [22, 23].

3. Classification of Dielectric Materials

The dielectric constant (k) of a material is basically the charge storage capability of that material. Materials can be classified into two categories: high-k materials and low-k materials [5]. Materials that have a value of dielectric constant more than silicon nitride, $k > 7$, are called high-k materials and the materials that have a dielectric constant value less than silicon dioxide, $k < 3.9$, are called low-k materials. The lowest value of k is of air, which is equal to unity. And the highest value of k is of relaxor ferroelectric, which is ~24000 at 1 KHz [4].

3.1. Applications of High-k and Low-k Materials. High-k materials can be used to develop efficient memory cells for high storage memory chips [43], to develop passive components like capacitors and supercapacitors [44]. They can be used for gate dielectrics in MOS transistors and TFTs [45]. Low-k materials find their applications in EMI Shielding [46], in the field of satellite communication, telecommunication in space [35], and high-speed IC packaging [47].

3.2. Demand for High-k Materials. Nowadays, electronic gadgets have become the fundamental need of daily life and with continuous thought of green evolution to minimize the use of paper, an efficient memory storage device plays a significant role [48]. These memory chips are made up of small capacitors and transistors as supporting circuitry [4]. The continuous efforts in the research and development in the field of material science make it possible to decrease the size of transistors and to accommodate a larger array on a single chip resulting in enhanced performance and storage. From equation (1), there are three approaches through which the storage capacity of a capacitor can be improved. First, the capacitance can be increased by increasing the area A, of capacitor's plates, but it will increase the device size also, which is not acceptable [26]. The second is to decrease the thickness of dielectric d or gap between capacitor's plates [27]. But dielectric breakdown strength of a material imparts constrain over a certain limit on the dielectric thickness, beyond that the material will either breakdown or the leakage current will start to flow through it. Therefore, the only possibility to enhance the performance and storage capacity of transistors/capacitors is to increase the value of the dielectric constant or to use a high-k material [28].

Thin-film transistors (TFTs) are the basic building block of every electronic gadget. TFTs are used in almost every flat panel display as a switch to drive the pixels. The resolution and clarity of the display depend upon the switching speed and performance of the TFTs [49–51]. The performance of a TFT is greatly influenced by the properties of its dielectric layer. The dielectric layer is responsible for the accumulation of charge in the channel and leakage current in the device [52, 53]. There is a fundamental limitation on the thickness of a silicon-based gate dielectric that the oxides having a thickness less than 2 nm suffer from direct tunnelling current or leakage current [54]. Therefore, high-k materials are required to overcome this problem. Due to these reasons, high-k materials are high in demand in the electronic industry and gain the attention of researchers [27]. Several materials like Ta_2O_5, Nb_2O_5, Y_2O_3, TiO_2, Al_2O_3, HfO_2, and ZrO_2 are available which have a value of dielectric constant varying from 10 to 100 [22, 55]. Water (H_2O) has $k = 80$ but it has very low dielectric strength. It cannot withstand high voltage. Hence, it cannot be used for practical applications [56]. So, there is a need to search new materials or synthesize new materials and tailor their properties as required. ZnO is one of the materials which is nontoxic and is safe for the

environment. It can offer greater dielectric constant after doping it with some other metals; hence, it can satisfy the need of energy storage devices.

4. Factors Affecting the Value of Dielectric Constant of a Material

Apart from frequency and temperature dependence, k of a material is also affected by its structural properties or microstructure:

(1) Crystallite size: if the size of the crystal of a material is large, then the value of k is also high. This is because a larger particle contains a greater number of dipoles which get aligned under the influence of the electric field and results in greater permittivity, thus a higher value of k [57, 58].

(2) Porosity: if the material is porous or has low density, then the value of k will be low [59]. A porous material is a dense material which is filled with random air pores. The value of permittivity or k of the material will decrease because the relative permittivity of air is much lower than the material itself; hence, with the increase in porosity, the overall value of k decreases [60].

(3) Composition and doping concentration: the composite materials consist of more than one material having different values of k. So, the resulting dielectric constant of the composite material will depend upon all the constituents. A dopant of low k will reduce the overall effective value of k of the composite material depending upon its percentage of concentration. A higher concentration of low-k dopant will result in more dip in the overall effective value of k of the material as compared to the lower concentration of dopant [61, 62].

(4) Defects: above room temperature, every material fundamentally has point defects to establish thermal equilibrium in the system:

(a) Surface defects: the surface of every material possesses inherent defects as it has a smaller number of bonds than the atoms in the bulk portion of the material. These loose bonds of the surface are called dangling bonds. If a material has more numbers of dangling bonds, that means it has a good density of charge carriers that will lead to large polarization [63].

(b) Vacancies: they exist in the system when there are some missing atoms in the crystal called vacancies. The existence of vacancies has a direct impact on the dielectric constant of the material [64]. The presence of vacancies in a material helps in trapping the charge carriers which generates large polarization, hence resulting in a high dielectric constant at low frequencies [65].

(c) Substitution defects: when some impurity atom or doping atom substitutes in the place of a host atom, it gives rise to substitution defects. These defects trap the charge carriers and produce large polarization, hence increasing the value of the dielectric constant at low frequencies [66].

(d) Grain boundaries: grain boundary is an interface that separates two grains in a polycrystalline material. It arises due to inhomogeneity in the surface of the material. If a material has a greater number of grain boundaries, then the value of k becomes high in the range of frequency, where interfacial polarization is active, as grain boundaries trap the charge carriers at the interfaces and do not allow them to move. Hence, they enhance the polarization and ultimately give rise to an increased value of dielectric constant at low frequencies [67].

5. Zinc Oxide (ZnO)

Zinc oxide (ZnO) is an n-type semiconductor that belongs to the II-VI group of the periodic table. It has been extensively studied and analysed by numerous researchers due to its outstanding properties, which include cost-effectiveness, wide availability, and nontoxic nature [68–70]. ZnO exhibits a wide bandgap of 3.37 eV. It also possesses a high exciton binding energy of 60 meV, which permits the device to operate at much higher voltage, frequency, and temperature than conventional semiconductors [71]. It shows a great performance of photocatalytic activities for the degradation of organic pollutants present in water, due to its ability to absorb almost the entire UV spectrum [72–74]. ZnO exhibits high quantum efficiency due to greater order of electron mobility 200–300 $cm^2 \cdot V^{-1} \cdot s^{-1}$ [75–77]. It has already been discussed that the dielectric properties of a material depend upon its structure. ZnO has structural defects like oxygen vacancies and zinc interstitials which are intrinsic to the synthesis process [66]. Huang et al. demonstrated that the number of oxygen vacancies that exist in the ZnO lattice exhibit a great impact on the relative permittivity and hence its dielectric properties [64]. ZnO is a polar molecule, hence possessing a permanent dipole moment, due to whichthe electronic polarization is high at low frequencies and decreases as the frequency of the applied field is increased [78]. Due to exceptional properties like great thermal stability, antimicrobial features, and biocompatibility, ZnO has proved to be a promising antibacterial agent [79–82]. ZnO in the food packaging industry has proved to improve the shelf life of food. It shows superb antibacterial properties for almost the entire range of bacteria including *Staphylococcus aureus* and *Escherichia coli* which is responsible for spoiling the food [83–86]. Due to the nontoxic nature of ZnO nanoparticles, these are biocompatible and hence safe for human beings [87–89].

Along with all these properties, it is ecofriendly, cheap, and widely available [90–92]. ZnO finds its application in drug delivery [93], targeted gene delivery, and tumour imaging [94]. It is used as an additive in ointments for various skin problems [95], as an antiseptic [96]. In the textile industry for developing a fabric which is UV radiation protected due to its UV absorption properties [97]. For food

packaging application, its antimicrobial properties help it to prevent the growth of bacteria which spoils the food and thus develop diseases [98, 99]. It also finds applications in devices like LED [100–104], TFTs [105, 106], memory cells [107], solar cells [108], photocatalyst [109], gas sensors [110], lasers [111], storage devices [112], and photodetectors [113].

5.1. Dielectric Constant of Bulk ZnO and ZnO Nanoparticles. The value of k of any material is a very important characteristic for various electronic applications like capacitors, transistors, dry electrodes, memory cells, passive components, and gate dielectrics. The k value for bulk ZnO ranges from 6 to 10 approximately at 1 MHz frequency and at room temperature [114]. Dielectric properties of ZnO have been examined by various researchers to find out the value of k of pure ZnO. Look et al. [115] found the value of the dielectric constant of bulk ZnO to be ≈ 8 at 1 MHz and at room temperature. Langton and Matthews [116] performed the dielectric studies of pure ZnO in the frequency range of 50 KHz to 25 MHz at 25°C and found the value of k for ZnO is 10.4 in the frequency range of 1 MHz to 10 MHz. As the frequency is increased above 10 MHz the value of k decreases and becomes 9.1 at 25 MHz.

It is well known that, with the increase in the ZnO layer thickness, the value of k increases at room temperature. At a fixed frequency, the k of ZnO varies with the variation of its thickness and temperature of operation [105]. It has been observed by Shashikant Sharma et al. that the dielectric constant increases with the increase in the film thickness of ZnO thin films, due to the quantum confinement effect [117]. The reduction in the value of dielectric constant of the thinner film is attributed to the powerful captivity of the smaller ZnO grains [118]. Table 1 and Figure 3 show the variation of dielectric constant as a function of the thickness of ZnO thin films at a fixed wavelength of 600 nm. The grade of crystallinity of ZnO thin films refines with the increase in thickness of films. With the increase in thickness of deposited films, the disorders like dislocation density, stress, and strain reduces. The dielectric behaviour of ZnO is ascribed to the defects like oxygen vacancies along with zinc interstitials [78]. In the optical properties, blue shift is observed with the decrease in thickness [119].

Lanje et al. [33] studied the dielectric properties of ZnO nanoparticles at room temperature and found the value of k to be 10.26 at 1 MHz. Literature disclosed that the value of k of a synthesized material depends upon various factors. The first factor is the size of nanoparticles of the synthesized material. Size dependence of the dielectric constant of ZnO nanoparticles has been studied in this paper. As shown in Table 2 and Figure 4, an increase in the value of k is observed with the increasing size of nanoparticles. It has been observed that the larger is the crystallite size of the particle, the higher is the value of k because the larger particle contains a greater number of dipoles which get aligned under the influence of the electric field, hence resulting in greater permittivity and higher value of k [57].

The dielectric constant of bulk zinc oxide is observed to be less than ZnO nanoparticles due to the fact that semiconductor nanoparticles exhibit a quantum confinement effect. As an outcome of their size in the nanometric range, the widening of the bandgap is caused when the spatial dimension is reduced. Quantum confinement regulates the band structure of the nanoparticles; hence, dielectric properties also change as the size of the nanoparticles is changed [124].

Pure ZnO has limited electronic and optical applications as pure ZnO has blue light emission which is the least eye sensitive colour and shows more scattering [125]. Pure ZnO has fixed and specific electric properties like bandgap, electron mobility, thermal conductivity, and exciton binding energy. The bandgap of ZnO can be tuned to a high or low value by adding some dopant. The addition of magnesium (Mg) into ZnO will increase the bandgap from 3.37 eV to 4 eV and the addition of cadmium (Cd) will decrease the bandgap to 3 eV [36]. Electrical and dielectric properties of ZnO depend upon the concentration of dopant. So, these

Table 1: Variation of the dielectric constant of ZnO thin films with the variation of film thickness at a fixed wavelength of 600 nm [118].

Thickness of the ZnO thin film (nm)	Value of dielectric constant
190	3.5
222	4.5
250	5
342	6

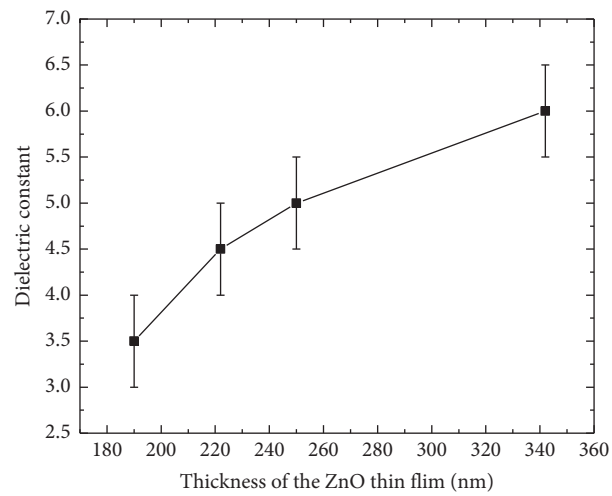

Figure 3: Variation of the dielectric constant of ZnO thin films with respect to film thickness.

Table 2: Variation of dielectric constant of ZnO nanoparticles with respect to the particle size.

Crystallite size of pure ZnO	Dielectric constant	References
15	5	[65]
19	14.78	[120]
19.97	9.7	[78]
22.84	18.5	[121]
33.03	17	[122]
55	45	[123]

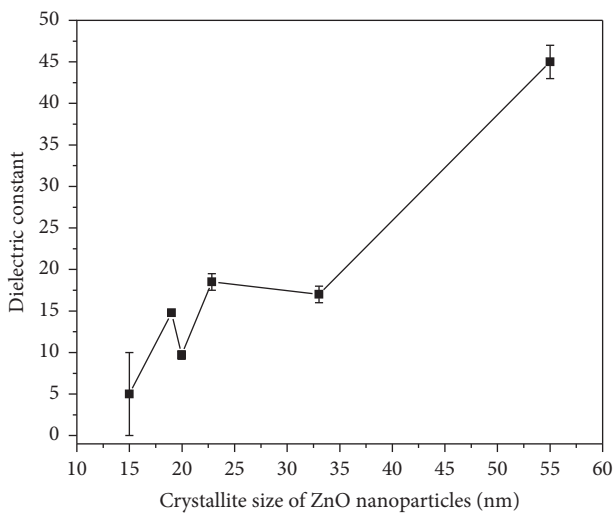

Figure 4: Variation of the dielectric constant of ZnO nanoparticles with respect to the crystallite size of ZnO nanoparticles.

properties can be tailored by adding some other materials in it and creating the composite.

6. Composites

When two or more materials which have quite different physical and chemical characteristics are combined in a manner that their properties remain distinct at the microscopic level, this type of material is called a composite material. Due to good physical strength and high melting point, high thermal conductivity composites find their applications in various industries [39].

6.1. Metal-Doped ZnO Nanocomposites and Their Applications. Two groups of metals, transition metal and rare earth metal, doped ZnO nanoparticles have been chosen for this review article. Ferromagnetism in transition metal (TM) doped ZnO is theoretically investigated by Sato and Katayama-Yoshida [126]. It turned out that most of the incomplete 3d shell metal ions can be used to produce room-temperature magnetism in ZnO, doped with transition metal [127]. In the case of rare earth (RE) doping, the 4f shell electrons are localized, exchange interactions are indirect as they occur via the 5d or 6s conduction electrons. However, the high orbital momentum leads to a high total magnetic moment per atom [128]. Other than introducing ferromagnetism transition metals, rare earth metal ions have been used by many researchers to dope ZnO. The doping thus modifies its optical, electrical, and dielectric properties by changing the bandgap and electronic structure of the composite material. Due to enhanced properties, it turned perfect for different technological applications like LED, TFTs, memory cells, solar cells, photocatalyst, gas sensors, lasing, storage devices, and photodetectors [129, 130]. Various researchers have synthesized different composites and have checked their dielectric properties.

6.1.1. Transition Metal-Doped ZnO. In this article transition metal-, Cr [121], Mn [57], Fe [78], Co [131, 132], Ni [122], and Cu [123], doped ZnO nanoparticles have been discussed for their dielectric studies. There are various factors that affect the value of the dielectric constant of a material like operating frequency, percentage of doping concentration, and atomic number of the dopant metal.

The first factor is the operating frequency: at low frequency, the value of k is high, and at high frequencies, the value becomes low for every material due to polarization phenomena [41, 133]. Figure 5 shows the graph which shows the variation of the dielectric constant of various transition metal-doped ZnO nanoparticles with respect to frequency in the range of 0 Hz to 10 MHz. Figure 5 shows that the value of the dielectric constant of every metal-doped ZnO is high at low frequencies since all four sources of polarization are active at low frequencies. ZnO is a polar molecule, so all the dipoles get aligned in the direction of the applied electric field and give rise to a higher value of k. As the frequency increases the value of k starts decreasing and becomes constant at a higher frequency because the dipoles are unable to align themselves with the changing direction of the applied field. Hence, the value of k decreases at high frequencies [120–123]. The phenomena of dielectric dispersion in such heterogeneous structures can be simply explained by the Maxwell–Wagner model [134–136]. According to this model, a dielectric medium is composed of conducting grains which are separated by resistive grain boundaries. The grains are effective at high frequencies and the grain boundaries are effective at low frequencies. Under the influence of the external field, the charge carriers easily transfer through grains but get trapped into the grain boundaries at low frequencies; this produces large polarization and high k. Among all the transition metals discussed in this article, Mn is showing a significant dielectric dispersion. The higher value of k at low frequencies can be explained based on interfacial polarization due to inhomogeneous structure, defects like oxygen vacancies, and grain boundary defects. Due to this reason, the value of k in Mn-doped ZnO is quite high at low frequencies; as the frequency increases, the value of k starts decreasing; and after a particular frequency, it becomes constant due to the fact that hopping between metal ions cannot follow the alternating field and are unable to align themselves in the direction of the electric field.

(1) Effect of Transition Metal Doping Concentration on Dielectric Constant. The second factor that affects the value of k is the composition and doping concentration. When ZnO nanoparticles are doped with metal ions, the crystal structure and microstructure of the nanoparticles change drastically which affects its chemical, electrical, mechanical, optical, and dielectric properties. This gives rise to various applications. The variations of the dielectric constant of different transition metal-doped ZnO nanoparticles have been discussed with respect to the percentage of doping concentration. As shown in Figure 6, some of the doped materials have a linearly decreasing trend with the increase in doping percentage and others have an increasing trend.

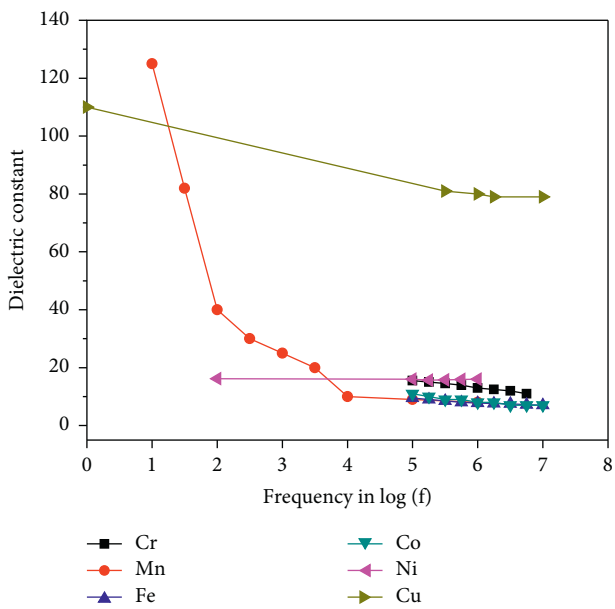

FIGURE 5: Variation of the dielectric constant of various transition metal-doped ZnO nanoparticles with respect to frequency.

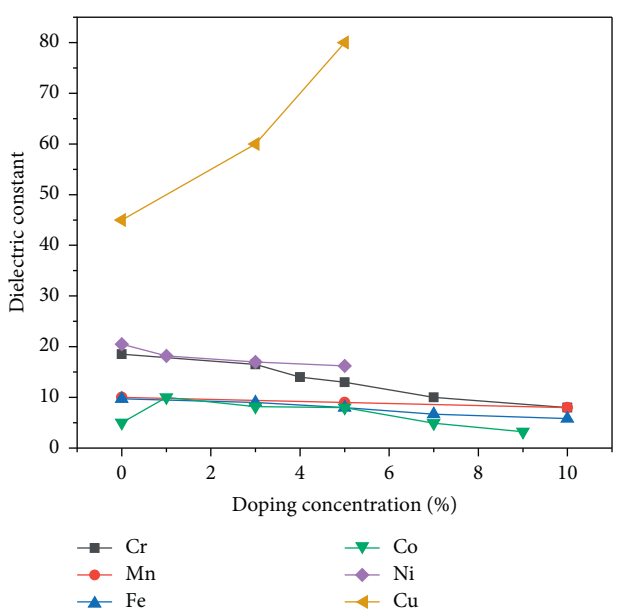

FIGURE 6: Variation of dielectric constant of transition metal-doped ZnO nanoparticles with respect to doping concentration at 1 MHz frequency.

Figure 6 shows the variation of k of transition metal-doped ZnO nanoparticles with different doping concentrations at 1 MHz frequency. The value of k decreases with the increase in the concentration of Cr, Mn, Fe, Co [132], and Ni into the ZnO nanoparticles. The doping of these metals prevents the growth of crystal grains and slows down the motion of a grain boundary. This reduction in motion of grain boundaries can be well explained with the Zener pinning effect [122]. As the ionic radius of these metals is smaller than Zn, it reduces the lattice parameters and crystallite size of the doped material [137, 138]. It has already been discussed that, with the reduction in crystallite size of nanoparticles the value of k decreases [57, 58]. Hence, a reduction in the size of nanoparticles leads to a reduction in the k value of doped material. When these metal ions are doped into ZnO at a lower concentration, the hopping mechanism between the metal ion and Zn^{2+} is predominant which results in a higher value of k. As the concentration is increased the metal ion in ZnO acts as a deep donor and decreases the concentration of intrinsic donors. It substitutes Zn^{2+} ions and produces charge imbalance around the dopants, which reduces the value of k. But in case of Cu, the value of k increases with the increase in the doping concentration; this is due to the abundance in electron exchange between Zn and Cu ions at all frequencies. Furthermore, it is seen that doping with Cu ions increases the grain size of doped material, so a large value of the dielectric constant may be attributed to the larger grain size and oxygen vacancies. Hence, it can be concluded that Cu doping enhances the polarization of ZnO nanoparticles.

(2) Effect of Atomic Number of Transition Metal on Dielectric Constant. The third factor is the atomic number of the dopant material. In order to compare the relative behaviour of various transition metal-doped ZnO nanocomposites, we have selected fixed doping concentration of 5% and fixed frequency of 1 MHz for every metal-doped ZnO nanocomposite. Figure 7 shows the variation of k value of various transition metal-doped ZnO nanoparticles at 5% doping and at 1 MHz frequency with respect to their atomic number. It has been observed that the value of k of various transition metal-doped ZnO nanoparticles increases exponentially as the atomic number increases from 24 to 29. The exceptional increase in the dielectric constant of Cu doped ZnO nanoparticles is due to the anomalous electronic configuration of Cu having atomic number 29, $3d^9 4s^2$ (ground state) having unfilled d orbital and fully filled s orbital. But instead of exhibiting this electronic configuration, it exhibits anomalous configuration having fully filled d orbital and partially filled s orbital, as the full 3d orbital is more stable than a full 4s orbital. This configuration causes the alignment of spin of the electrons resulting in long-range ferromagnetic order in Cu doped ZnO. Doping at the 3d transition metal site by transition metal ions in ZnO lattice has observed a variety of magnetic and electronic orders with spatially correlated charge spin and orbital degree of freedom. Hence, enhanced dielectric constant is observed.

6.1.2. Rare Earth Metal-Doped ZnO. Rare earth metal-, Ce [139], Gd [130, 140], La [141], Nd [142], Ho [143], Er [144], and Tm [145], doped ZnO nanoparticles have been discussed for their dielectric studies in this article.

Figure 8 shows the variation of the dielectric constant of various rare earth metal-doped ZnO nanoparticles with respect to frequency in the range of 0 Hz to 10 MHz. In the graph, it has been observed that the value of the dielectric constant of every rare metal-doped ZnO is high at low frequencies since all four sources of polarization are active at

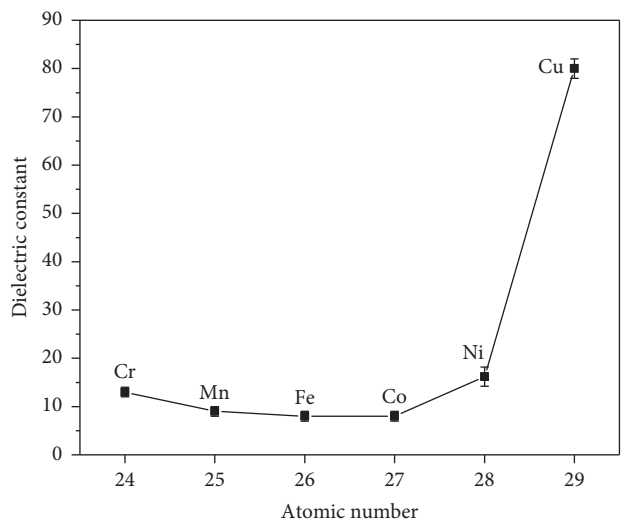

Figure 7: Variation of the dielectric constant of various transition metal-doped ZnO nanoparticles at 5% doping and at 1 MHz frequency with respect to their atomic number.

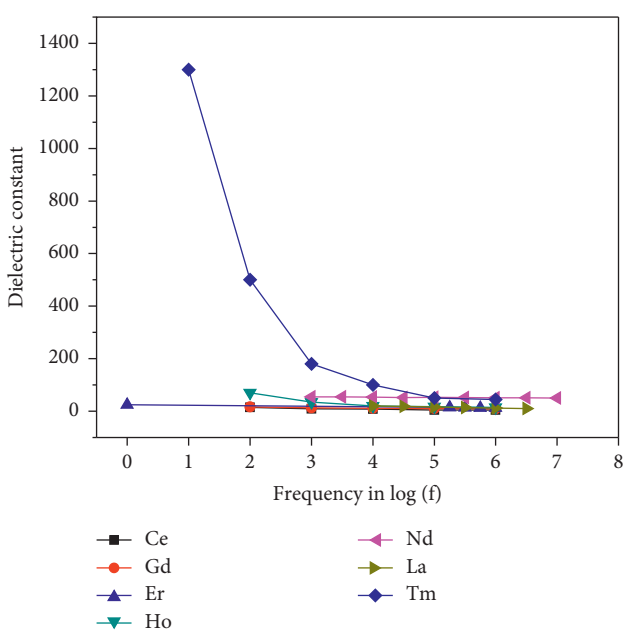

Figure 8: Variation of the dielectric constant of various rare earth metal-doped ZnO nanoparticles with respect to frequency.

low frequencies. ZnO is a polar molecule so all the dipoles get aligned in the direction of the applied electric field and give rise to a higher value of k. As the frequency increases, the value of k starts decreasing and after a particular frequency it becomes constant, as hopping between different metal ions cannot follow the alternating field. Hence, the value of k decreases at high frequencies [141–145]. The phenomena of dielectric dispersion are attributed to the Maxwell–Wagner model. Among all the rare earth metals discussed in this article, Tm is showing a significant dielectric dispersion. The value of k is very high at low frequencies because Tm is highly polarizable and a higher value of k at low frequencies can be explained based on interfacial polarization due to inhomogeneous structure and defects like oxygen vacancies and grain boundary defects.

(1) Effect of Rare Earth Metal Doping Concentration on Dielectric Constant. Figure 9 shows the variation of k for some rare earth metal-doped ZnO nanoparticles with different doping concentrations at 1 MHz frequency. In Ce-doped ZnO nanoparticles, initially, the value of k decreases due to the high density of defects. But a further increase in doping concentration increases the value of k due to less electronegativity of Ce than Zn that makes the ionic bonds weaker [139]. The dielectric constant of Gd-doped ZnO nanoparticles decreases with the increase in doping concentration due to a decrease in relaxation time where ionic and orientational polarization are closely connected with each other. Gd acts as an acceptor and absorbs free charge carriers, hence decreasing the value of k [130].

A larger ionic radius of Nd^{3+} ions substituted for Zn^{2+} ions in Nd-doped ZnO indicates local distortion in the doped ZnO lattice, due to which, initially, the value of k increases with doping but as the doping concentration is increased further, the sample becomes porous and hence the value of k starts decreasing, as these pores get filled with air which has low dielectric constant, hence decreasing the overall dielectric constant of the doped sample [142].

The value of k in Ho-doped ZnO increases monotonically with the increase in doping concentration. This is because the decrease in columbic interaction causes an increase in exciton binding energy which leads to an increase in the value of k [143]. The value of k in Er-doped ZnO nanoparticles varied according to its size. Initially, up to 3% of doping, the value of k decreased and then it increased again because initially the nanoparticles had a rod-like structure and with the further increase in concentration, it started to change into a plate-like structure. Hence, the value of k started to increase with the increase in the concentration of Er [144].

(2) Effect of Atomic Number of Rare Earth Metal on Dielectric Constant. Figure 10 shows the variation of k value of various rare earth metal-, La [141], Ce [139], Nd [142], Gd [140], Er [144], and Tm [145], doped ZnO nanoparticles at 5% doping and at 1 MHz frequency with respect to their atomic number. It has been observed that the value of k of various rare earth metal-doped ZnO nanoparticles increases exponentially as atomic number increases from 57 to 69. Significant enhancement in the dielectric constant of Tm-doped ZnO is due to the anomalous electronic configuration of Tm having atomic number 69, $4f^{13}\ 6s^2$ (ground state) having unfilled f orbital and fully filled s orbital. But instead of exhibiting this electronic configuration, it exhibits anomalous configuration having fully filled f orbital and partially filled s orbital as the full 4f orbital is more stable than a full 6s orbital. This configuration causes the alignment of the spin of the electrons resulting in long-range ferromagnetic order in Tm doped ZnO. Doping at the posttransition metal site by rare earth ions in ZnO lattice has observed a variety of magnetic and electronic orders with spatially correlated

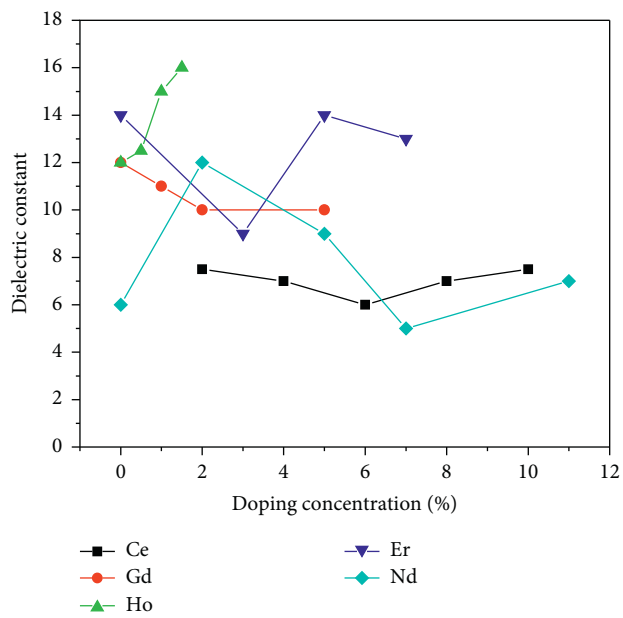

Figure 9: Variation of dielectric constant of rare earth metal-doped ZnO nanoparticles with respect to doping concentration at 1 MHz frequency.

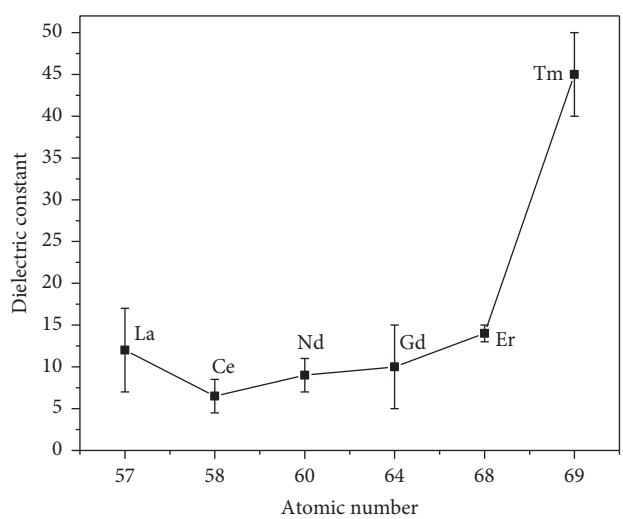

Figure 10: Variation of the dielectric constant of various rare earth metal-doped ZnO nanoparticles at 5% doping and at 1 MHz frequency with respect to their atomic number.

charge spin and orbital degrees of freedom. Hence, large ferromagnetism and enhanced dielectric constant are observed.

Table 3 expresses the value of k of various metal-doped ZnO nanoparticles for 5% doping at an operating frequency of 1 MHz and their respective electronic applications. The graph in Figure 11 shows that Cu among transition metals and Tm among all the rare earth metals discussed in this article attain the highest value of k, 80 and 45, respectively, at 5% doping and at 1 MHz frequency.

7. Polymer

Polymers are of great attraction for researchers due to various interesting properties like low cost, flexibility, lightweight, easy processing, and wide range of operating frequency [35]. Petrochemical plastics were used widely in consumer-based products, food packaging, lightings, automobiles, and many electronic applications such as printed circuit board (PCB) due to their easy modification of shape, structure, and properties [146].

7.1. Polymer Nanocomposites. The small size particles called nanofillers are used to distribute into the polymer matrix which acts as a flexible base matrix which gives rise to a polymer nanocomposite [147, 148]. So, the properties of a composite material are greatly affected by the choice of polymer matrix and the nanofiller. Polymer-based nanocomposites have many applications in the field of medical and engineered technology due to their good electron transport and mechanical and optical properties [149, 150]. They are good aspirants for energy storage applications. Degradation resistance improved thermal and mechanical properties along with improved dielectric breakdown strength being the added advantages of polymer nanocomposites [151, 152].

7.1.1. Polymer-Based ZnO Nanocomposites. A lot of work is done to explore the dielectric and electrical properties of polymer nanocomposites. Figure 12 shows the variation of the dielectric constant of various polymer-based ZnO nanocomposites with respect to frequency in the range of 0 Hz to 1 MHz. In the graph, it has been observed that the value of the dielectric constant of every polymer-based ZnO nanocomposite is high at low frequencies because all four sources of polarization are active at low frequencies and ZnO is a polar molecule, so all the dipoles get aligned in the direction of applied electric field and thus give rise to a higher value of k. As the frequency increases, the value of k starts decreasing and after a particular frequency, it becomes constant since dipoles cannot follow the alternating field and are unable to align themselves in the direction of the electric field. Hence, the value of k decreases at high frequencies [141–145]. The dielectric dispersion in the case of polymer nanocomposites is attributed to Maxwell–Wagner–Sillars (MWS) effect which represents the collection of charge at the interfaces of materials having different conductivity which leads to increased polarizability in the composite material [153].

In ethylene-vinyl acetate (EVA)/ZnO nanocomposite, the larger value of dielectric constant at low frequencies is due to the space change polarization which arises because of impurities and defects present in the nanocomposite [38]. In case of polyvinyl chloride (PVC)/ZnO nanocomposite, the value of dielectric constant is high at low frequencies and the value starts decreasing as the frequency is increased. This is

Table 3: Various metal-doped ZnO nanoparticles and their potential applications.

Metal	Doping (%)	Frequency (MHz)	Dielectric constant of metal-doped ZnO nanoparticles	Applications
Ce	5	1	6.5	High-frequency device applications
Fe	5	1	8	Nano-optoelectronic applications
Co	5	1	8	Optical applications
Mn	5	1	9	Spintronic applications
Nd	5	1	9	Pressure sensors, piezoelectric nanogenerators for energy harvesting
La	5	1	12	Storage applications
Cr	5	1	13	LEDs, optoelectronic devices
Er	5	1	14	High-frequency device applications
Ni	5	1	16.2	Optoelectronic applications
Tm	5	1	45	Dye-sensitized solar cell applications.
Cu	5	1	80	High dielectric constant applications

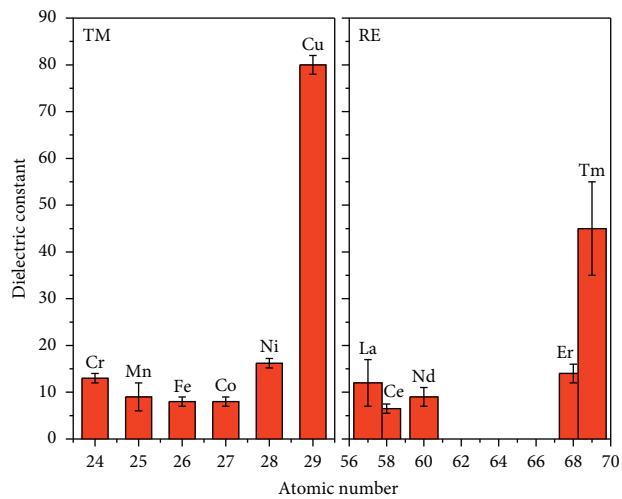

Figure 11: Dielectric constant of various metal-doped ZnO nanoparticles for 5% doping at 1 MHz frequency.

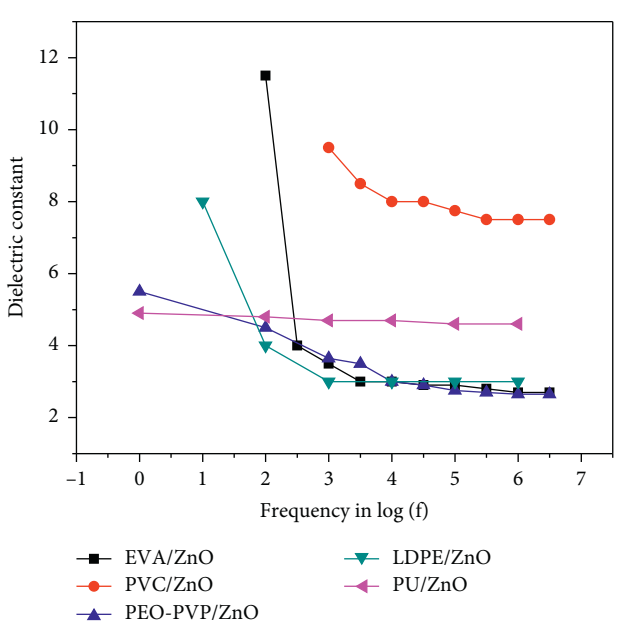

Figure 12: Variation of the dielectric constant of various polymer-based ZnO nanocomposites with respect to frequency.

due to the reduction in orientational polarization at high frequencies [154]. In poly(ethylene oxide) (PEO) poly(vinylpyrrolidone) (PVP) blend matrix PEO-PVP/ZnO nanocomposite, the larger value of k at low frequencies is attributed to the interfacial polarization in the nanocomposite material [155]. In case of low-density polyethylene (LDPE)/ZnO nanocomposite, the value of dielectric constant is higher at low frequencies due to the presence of interfacial polarization and as the frequency increases, the value of k decreases as interfacial polarization is no longer active at high frequencies [156].

Figure 13 shows the variation of k of the above-discussed polymer ZnO nanocomposites with different doping concentrations at 1 KHz frequency. In every polymer nanocomposite, the value of k increases as the concentration of ZnO nanofiller is increased, this is because these polymers have a low dielectric constant as compared to the ZnO nanoparticles. So, when a composite is prepared with ZnO as a nanofiller, the effective value of k of the polymer nanocomposite is increased. And as the concentration is increased, the effective value of k further increases. Along with this, homogeneous dispersion of nanofillers in the polymer matrix are required to ensure that there is no agglomeration

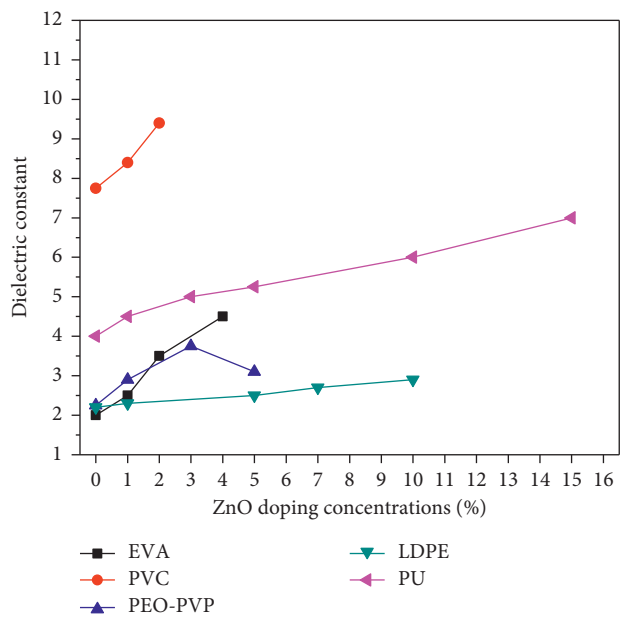

Figure 13: Variation of the dielectric constant of various polymer-based ZnO nanocomposites with respect to doping concentration at 1 KHz frequency.

of nanoparticles that provide tunnelling, hence reducing the dielectric breakdown strength of polymer nanocomposite [157]. In case of PEO-PVP/ZnO nanocomposite, the value of k increases up to 3% filler concentration due to the fact that the dielectric constant of PEO-PVP is less than ZnO nanoparticles hence with the addition of ZnO, there is an increase in the effective dielectric constant of the polymer nanocomposite. But after that at 5%, it started decreasing which may be due to the electrostatic interaction between functional groups of polymer blend and ZnO nanoparticles resulting in a reduction of the orientation of dipoles, hence resulting in reduced dielectric polarization in the nanocomposite. In case of PU/ZnO and LDPE/ZnO nanocomposite, the value of k increases very linearly with the increase in the concentration of ZnO nanoparticles. But in case of EVA/ZnO and PVC/ZnO nanocomposite, an abrupt change in k is observed with the increase in the concentration of ZnO nanoparticles. Due to the lack of availability of data points in the literature, a conclusion cannot be made if the values of the dielectric constant will increase exponentially or like a parabola with the increase in concentration. Hence, in case of polymer-based ZnO nanocomposites, there is still room available to study the effect of concentration on the dielectric properties.

7.1.2. Applications of Polymer Nanocomposites. Polymer nanocomposites are used in several electronic applications due to their promising electrical, dielectric, optical, and mechanical properties. Polymer nanocomposites are used in the devices like organic field effect transistors [158–161], gas sensors [162–166], solar cells [167–171], high power and high storage density capacitors and supercapacitors [172–177], electromagnetic interference shielding [178], thermochromic and electrochromic devices [179], electronic antenna [180], optoelectronic devices [181], high capacity memory devices [182], insulating materials [183, 184], nanodielectric applications [185, 186], and printed circuit board [187–189].

7.2. Biodegradable Polymers. Although polymer nanocomposites show very good and promising dielectric properties and enhanced dielectric breakdown strength, the biggest disadvantage is the toxic nature of petroleum-based polymers. When the devices or products made up of petroleum-based polymers are disposed of, they contaminate the environment, which is harmful to living organisms and human beings [97]. So, the electronic products are required to be made up of a material which is biocompatible and biodegradable and is safe for human beings along with other living organisms, hence promoting the green technology.

7.2.1. Biodegradable Polymer Nanocomposites. Nowadays, biofriendly or echo-friendly materials are high in demand in every field as they are nontoxic [38,190]. Biodegradable polymer nanocomposite is a category of materials that have very interesting properties compared to pure biodegradable polymers and old composites. They have all the properties and advantages of polymers, but an additional advantage is that they are biodegradable. Biodegradable polymers are made up of living organism's protein and DNA. Biodegradable polymers nanocomposites are doing very well in various fields. They are used for food packaging to improve the shelf life of food [191–193], as a photocatalyst to purify water [194, 195], cancer treatments [196–198], drug delivery in the medical field [199–201], antimicrobial activities [202–204], tissue engineering [205], and sensors [206, 207].

Various researchers have made use of biodegradable polymers to develop some new biodegradable nanocomposites. There are various biodegradable polymers like poly(3-hydroxybutyrate) (PHB), polylactic acid (PLA), polycaprolactone (PCL), poly(butylene succinate) (PBS), poly(butylene adipate-co-terephthalate) (PBAT), poly(3-hydroxybutyrate-co-3-hydroxyvalerate) (PHBV), (poly-lactide-co-glycolide) (PLGA), chitosan, cellulose, and gluten.

These are 100% biodegradable polymers, and they have several applications in different areas. Polyhydroxyalkanoates (PHA) is a class of polymers which is made from renewable sources synthesized by bacteria from carbon and oxygen [208, 209]. In this class, PHB is the most widely studied and useful biopolymer. But it has some disadvantages like it is very brittle, cost of production is very high, it does not have any resistance to thermal degradation, and it has a high melting point, due to which it is not suitable for industrial applications [209–212].

7.2.2. Biodegradable Polymer-Based ZnO Nanocomposites and Their Applications. All the LEDs emit UV radiations in addition to visible light which is very harmful to the living organisms [213]. Poly(3-hydroxybutyrate-co-3-hydroxyvalerate) (PHBV) polymer/ZnO nanocomposite provides

the absorption of entire UV region. This enables the material to be used as an encapsulation material for LEDs [190]. This material absorbs all the UV radiation spectra and emits only visible light. The PHB-ZnO nanocomposite material can be used in textile industry for UV blocking applications [214–216]. The same material can also be used to manufacture printed circuit boards (PCB) which are nontoxic and do not contaminate the environment when disposed off [190]. The material is good for antibacterial applications [217]. PHBV and ZnO nanocomposite is very good for food packaging applications [218–221]. Enhanced value of dielectric constant of polylactide acid (PLA) and poly(butylene adipate-co-terephthalate) (PBAT) with graphene nanocomposites is useful for EMI shielding applications [222, 223]. Poly(butylene succinate) (PBS) and ZnO nanocomposite films are very suitable material for food packaging to improve the shelf life of packed food due to its good antimicrobial and mechanical properties [224].

Enhancement in mechanical, antimicrobial, and dielectric properties of chitosan/ZnO nanocomposite films with the increase of ZnO concentration is very good for food packaging applications [225–227]. Chitosan-ZnO/polyaniline ternary nanocomposite material is recommended for storage of charge in supercapacitors [228]. Chitosan is a nontoxic, biocompatible, and biodegradable polymer which is obtained from shells of lobsters or crabs and also in the cell walls of fungi. It has antimicrobial and UV protection properties as well [229–231]. The enhanced photoluminescence intensity of the Chitosan capped ZnO nanocomposite makes the material suitable for display devices and biomedical applications [125, 232, 233].

7.3. Future Aspects. The field of biodegradable nanocomposites is still being explored because it has a lot more to give to the society and electronic industry:

(1) Higher value of dielectric constant for ZnO nanoparticles can be achieved by doping it with some rare earth metals or transition metals. As ZnO is a nontoxic material, it is safe for the human being and the environment to be used in electronic products like thin-film transistors, memory cells, and high-speed integrated circuits.

(2) Keeping in mind environmental safety there is a need to design and synthesize nontoxic and biodegradable dielectric material for energy storage applications. Hence, ZnO-based biodegradable polymer nanocomposites can be used as a dielectric material for developing energy storage devices like capacitors to enhance their energy density.

(3) To enhance the energy storage density, a multilayered structure of ZnO-based biodegradable polymer nanocomposite can be developed to achieve a higher value of energy density.

(4) A sandwiched structure of ZnO-based biodegradable polymer nanocomposites with different concentrations of ZnO nanoparticles as filler in the biodegradable polymer as the base matrix can be used to enhance the energy density of the material further.

8. Conclusion

Dielectric constant is a very important factor of a material which determines its applications in the electronic industry as a capacitor, thin-film transistor, memory devices, high-speed IC packaging, and EMI shielding. ZnO is one of the most demanded materials in the electronic industry due to its very attractive properties like wide availability, nontoxicity, and cost-effectiveness. Nanocomposites of ZnO have been explored by various researchers. Two groups of metals, transition metal and rare earth metal, have been chosen to be a dopant in ZnO for this review. The literature revealed that the value of the dielectric constant of a synthesized material depends upon various factors. The first factor is the size of nanoparticles of synthesized material, the larger the size of nanoparticles, the higher will be the value of dielectric constant due to the fact that larger particle contains a greater number of dipoles which get aligned under the influence of the electric field. Second, the thickness of films also affects the value of the dielectric constant. The value increases with the increase in the film thickness of ZnO thin films due to the quantum confinement effect. Third, the density of the material: if the material is porous, the value of the dielectric constant will be less and if the material is of high density, the value of the dielectric constant will be high. Fourth, operating frequency: at low frequency the value of the dielectric constant is high and at high frequencies, the value becomes low for every material since all four sources of polarization are active at low frequencies, and at high frequencies, the dipoles are unable to align themselves with the changing direction of the applied field. Fifth, the defects in the material, such as oxygen vacancies, zinc interstitials, and inhomogeneities like grain boundaries, are inherent to the synthesis process of the material. The higher the defects, the higher will be the value of dielectric constant of the material at low frequencies.

Among all the metals discussed in this article, transition metal Mn and rare earth metal Tm are showing a significant dielectric dispersion. The higher value of k at low frequencies can be explained based on interfacial polarization due to inhomogeneous structure and defects such as oxygen vacancies and grain boundary defects. The exponential increase in the dielectric constant of Cu among transition metals and Tm among rare earth metal-doped ZnO at the same doping concentration is due to the anomalous electronic configuration.

Petroleum-based polymer ZnO nanocomposites are also observed to show promising dielectric properties. But they lag due to their toxic nature which contaminates the environment when they are disposed of. Biodegradable ZnO nanocomposites are explored by various researchers which shows good mechanical, antibacterial, antimicrobial, and dielectric properties which enabled these materials to be used as food packaging materials and in various medical

applications. Still, there is much room available to study the effect of filler concentration on the dielectric properties of polymer ZnO nanocomposites. To experience all the advantages of a polymer material along with the nontoxicity, the dielectric properties of biodegradable ZnO nanocomposites need to be explored in depth so that these materials can be used in electronic applications as storage materials and many more electronic applications. Hence, electronic products need to be made up of the material, which is biocompatible, biodegradable, and safe for living organisms as well as human beings, hence promoting green technology.

Data Availability

The data used to support the findings of this study in the manuscript are available from the corresponding author upon request.

Conflicts of Interest

The authors declare that they have no conflicts of interest.

Acknowledgments

The authors are thankful to the Electronics and Communication Engineering Department of UIET, Punjab University, for providing the facilities to carry out this research work.

References

[1] W. R. Tinga and S. O. Nelson, "Dielectric properties of materials for microwave processing-tabulated," *Journal of Microwave Power*, vol. 8, no. 1, pp. 23–65, 1973.

[2] X. Huang and P. Jiang, "Core-shell structured high-*k* polymer nanocomposites for energy storage and dielectric applications," *Advanced Materials*, vol. 27, no. 3, pp. 546–554, 2015.

[3] J. Robertson and R. M. Wallace, "High-*K* materials and metal gates for CMOS applications," *Materials Science and Engineering: R: Reports*, vol. 88, pp. 1–41, 2015.

[4] R. Singh and R. K. Ulrich, "High and low dielectric constant materials," *The Electrochemical Society Interface*, vol. 8, p. 26, 1999.

[5] H. S. Nalwa, *Hand Book of Low and High Dielectric Constant Materials and Their Applications*, Academic Press, Ibaraki, Japan, 1999.

[6] S. Park, C.-H. Kim, W.-J. Lee, S. Sung, and M.-H. Yoon, "Sol-gel metal oxide dielectrics for all-solution-processed electronics," *Materials Science and Engineering: R: Reports*, vol. 114, pp. 1–22, 2017.

[7] X. Huang, Z. Pu, L. Tong, Z. Wang, and X. Liu, "Preparation and dielectric properties of surface modified TiO_2/PEN composite films with high thermal stability and flexibility," *Journal of Materials Science: Materials in Electronics*, vol. 23, no. 12, pp. 2089–2097, 2012.

[8] R. P. Ortiz, A. Facchetti, and T. J. Marks, "High-*k* organic, inorganic, and hybrid dielectrics for low-voltage organic field-effect transistors," *Chemical Reviews*, vol. 110, no. 1, pp. 205–239, 2010.

[9] V. S. Jahnavi, S. K. Tripathy, and A. V. N. Ramalingeswara Rao, "Structural, optical, magnetic and dielectric studies of SnO_2 nano particles in real time applications," *Physica B: Condensed Matter*, vol. 565, pp. 61–72, 2019.

[10] S. Sarmah and A. Kumar, "Optical properties of SnO_2 nanoparticles," *Indian Journal of Physics*, vol. 84, no. 9, pp. 1211–1221, 2010.

[11] E. Pradyumna, N. Sreelekha, D. Amaranatha Reddy, K. R. Gunasekhar, and K. Subramanyam, "Dopant induced room temperature ferromagnetism in spintronic SnO_2: Co nanoparticles," *The International Journal of Advanced Engineering and Nano Technology*, vol. 2, p. 22, 2015.

[12] Q. Zhao, L. Ma, Q. Zhang, C. Wang, and X. Xu, "SnO_2-Based nanomaterials: synthesis and application in lithium-ion batteries and supercapacitors," *Journal of Nanomaterials*, vol. 2015, Article ID 850147, 15 pages, 2015.

[13] X. W. Lou, Y. Wang, C. Yuan, J. Y. Lee, and L. A. Archer, "Template-free synthesis of SnO_2 hollow nanostructures with high lithium storage capacity," *Advanced Materials*, vol. 18, no. 17, pp. 2325–2329, 2006.

[14] H. J. Van Daal, "The static dielectric constant of SnO_2," *Journal of Applied Physics*, vol. 39, no. 9, pp. 4467–4469, 1968.

[15] A. Ahmed, P. Tripathi, M. Naseem Siddique, and T. Ali, "Microstructural, optical and dielectric properties of Al-incorporated SnO2 nanoparticles," *IOP Conference Series: Materials Science and Engineering*, vol. 225, Article ID 012173, 2017.

[16] C. Madhu, I. Kaur, and N. Kaur, "Synthesis and investigation of photonic properties of surface modified ZnO nanoparticles with imine linked receptor as coupling agent- for application in LEDs," *Journal of Materials Science: Materials in Electronics*, vol. 28, no. 9, pp. 6388–6398, 2017.

[17] T. Xiao, B. Heng, X. Hu, and Y. Tang, "In situ CVD synthesis of wrinkled scale-like carbon arrays on ZnO template and their use to supercapacitors," *The Journal of Physical Chemistry C*, vol. 115, no. 50, pp. 25155–25159, 2011.

[18] S. Shi, X. Zhuang, B. Cheng, and X. Wang, "Solution blowing of ZnO nanoflake-encapsulated carbon nanofibers as electrodes for supercapacitors," *Journal of Materials Chemistry A*, vol. 1, no. 44, pp. 13779–13788, 2013.

[19] D. Bresser, F. Mueller, M. Fiedler et al., "Transition-metal-doped zinc oxide nanoparticles as a new lithium-ion anode material," *Chemistry of Materials*, vol. 25, no. 24, pp. 4977–4985, 2013.

[20] J. Wang, R. Chen, L. Xiang, and S. Komarneni, "Synthesis, properties and applications of ZnO nanomaterials with oxygen vacancies: a review," *Ceramics International*, vol. 44, no. 7, pp. 7357–7377, 2018.

[21] z. Guang, *Handbook of Advanced Dielectric, Piezoelectric and Ferroelectric Materials Synthesis Properties and Applications*, Woodhead Publishing, Sawston, UK, 2008.

[22] H. Treichel, A. Mitwalsky, G. Tempel et al., "Deposition, annealing and characterisation of high-dielectric-constant metal oxide films," *Advanced Materials for Optics and Electronics*, vol. 5, no. 3, pp. 163–175, 1995.

[23] P. Lunkenheimer, S. Krohns, S. Riegg, S. G. Ebbinghaus, A. Reller, and A. Loidl, "Colossal dielectric constants in transition-metal oxides," *The European Physical Journal Special Topics*, vol. 180, no. 1, pp. 61–89, 2009.

[24] K. Meher and K. B. R. Varma, "Colossal dielectric behavior of semiconducting Sr2TiMnO 6 ceramics," *J. Appl. Phys.*vol. 105, 2009.

[25] K. C. Kao, "Dielectric phenomena in solids: with emphasis on physical concepts of electronic processes," *Electric*

Polarization and Relaxation, Dielectric Phenomena in Solids, vol. 10, pp. 41–114, 2004.

[26] P. Balk, "Dielectrics in microelectronics - problems and perspectives," *Journal of Non-crystalline Solids*, vol. 187, pp. 1–9, 1995.

[27] H. Treichel, E. Eckstein, and W. Kern, "New dielectric materials and insulators for microelectronic applications," *Ceramics International*, vol. 22, no. 5, pp. 435–442, 1996.

[28] S. Vyas, "A short review on: optimization techniques of ZnO based thin film transistors," *Chinese Journal of Physics*, vol. 56, no. 1, pp. 117–124, 2018.

[29] P. Capacitor: Chapter 5 Capacitance and Dielectrics.

[30] J. G. Kirkwood, "On the theory of dielectric polarization," *The Journal of Chemical Physics*, vol. 4, no. 9, pp. 592–601, 1936.

[31] R. Dorey, "Microstructure-property relationships," *Ceramic Thick Films for MEMS and Microdevices*, vol. 39, pp. 85–112, 2012.

[32] V. Sundar, R. E. Newnham, and R. E. Newnham, "Electrostriction and polarization," *Ferroelectrics*, vol. 135, no. 1, pp. 431–446, 1992.

[33] A. S. Lanje, S. J. Sharma, R. S. Ningthoujam, J.-S. Ahn, and R. B. Pode, "Low temperature dielectric studies of zinc oxide (ZnO) nanoparticles prepared by precipitation method," *Advanced Powder Technology*, vol. 24, no. 1, pp. 331–335, 2013.

[34] P. Boussard, P. E. M. Siegbahn, and U. Wahlgren, "Cluster models of zinc oxide including ionic and covalent effects," *Adsorption on Ordered Surfaces of Ionic Solids and Thin Films*, vol. 33, pp. 192–205, 1993.

[35] M. L. Singla, R. Sehrawat, N. Rana, and K. Singh, "Dielectric behaviour of emeraldine base polymer-ZnO nanocomposite film in the low to medium frequency," *Journal of Nanoparticle Research*, vol. 13, no. 5, pp. 2109–2116, 2011.

[36] K. Omar, M. D. Johan Ooi, and M. M. Hassin, "Investigation on dielectric constant of zinc oxide," *Modern Applied Science*, vol. 3, pp. 110–116, 2009.

[37] I. Latif, E. AL-Abodi, J. Al Khafagi, and K. Al, "Preparation, characterization and electrical study of (carboxymethylated polyvinyl alcohol/ZnO) nanocomposites," *American Journal of Polymer Science*, vol. 2, no. 6, pp. 135–140, 2013.

[38] J. Sebastian, E. T. Thachil, J. J. Mathen et al., "Enhancement in the electrical and thermal properties of ethylene vinyl acetate (EVA) co-polymer by zinc oxide nanoparticles," *Open Journal of Composite Materials*, vol. 05, no. 03, pp. 79–91, 2015.

[39] A. F. Mansour, S. F. Mansour, and M. A. Abdo, "Enhancement of structural and electrical properties of ZnO/PVA nanocomposites," *IOSR Journal of Applied Physics*, vol. 7, pp. 97–106, 2015.

[40] H. Singh, A. Bharti, N. Goyal, and P. S. Gill, "Metallic/chalcogen dual phase effects on dielectric relaxations, resonance and spectroscopic impedance in amorphous chalcopyrite CuxInyGa10Se70−xTe20−y thin films," *Journal of Materials Science: Materials in Electronics*, vol. 29, no. 17, pp. 14406–14415, 2018.

[41] A. K. Jonscher, "Dielectric relaxation in solids," *Journal of Physics: Applied Physics*, vol. 32, 1999.

[42] K. S. Cole and R. H. Cole, "Dispersion and absorption in dielectrics I. alternating current characteristics," *The Journal of Chemical Physics*, vol. 9, no. 4, pp. 341–351, 1941.

[43] J. Charles Pravin, D. Nirmal, P. Prajoon, N. Mohan Kumar, and J. Ajayan, "Investigation of 6T SRAM memory circuit using high-k dielectrics based nano scale junctionless transistor," *Superlattices and Microstructures*, vol. 104, pp. 470–476, 2017.

[44] W. Raza, F. Ali, N. Raza et al., "Recent advancements in supercapacitor technology," *Nano Energy*, vol. 52, pp. 441–473, 2018.

[45] D.-B. Ruan, P.-T. Liu, Y.-C. Chiu et al., "Investigation of low operation voltage in ZnSnO thin-film transistors with different high-*k* gate dielectric by physical vapor deposition," *Thin Solid Films*, vol. 660, pp. 885–890, 2018.

[46] A. Abolghasemi Mahani, S. Motahari, and V. Nayyeri, "Synthesis, characterization and dielectric properties of one-step pyrolyzed/activated resorcinol-formaldehyde based carbon aerogels for electromagnetic interference shielding applications," *Materials Chemistry and Physics*, vol. 213, pp. 492–501, 2018.

[47] S. Devaraju, M. R. Vengatesan, M. Selvi, J. K. Song, and M. Alagar, "Mesoporous silica reinforced cyanate ester nanocomposites for low k dielectric applications," *Microporous and Mesoporous Materials*, vol. 179, pp. 157–164, 2013.

[48] M. Kobayashi, "More than moore," *The Journal of The Institute of Image Information and Television Engineers*, vol. 70, no. 3, pp. 324–327, 2016.

[49] F. Wu: P-25 Improved electrical performance of organic thin-film transistors with modified high- K dielectrics.

[50] A. Subramaniyam, C. Robinson, and A. John, "Fabrication of thin film transistor using high *K* dielectric materials," *International Journal of Engineering and Computer Science*, vol. 3, no. 4, 2017.

[51] D. J. Dimaria, D. Arnold, and E. Cartier, "Degradation and breakdown of silicon dioxide films on silicon," *Applied Physics Letters*, vol. 61, no. 19, pp. 2329–2331, 1992.

[52] Y. Y. Yu, A. H. Jiang, and W. Y. Lee, "Organic/inorganic nano-hybrids with high dielectric constant for organic thin film transistor applications," *Nanoscale Research Letters*, vol. 11, p. 488, 2016.

[53] H. Zulkefle, L. N. Ismail, R. A. Bakar, M. H. Mamat, and M. Rusop, "Enhancement in dielectric constant and structural properties of sol-gel derived MgO thin film using ZnO/MgO multilayered structure," *International Journal of Applied Physics and Mathematics*, vol. 2, pp. 38–043, 2012.

[54] J. Li and X. Bi, "Temperature- and frequency-dependent dielectric behaviour of insulator/semiconductor (Al2O3/ZnO) nanolaminates with various ZnO thicknesses," *Journal of Physics D: Applied Physics*, vol. 49, 2016.

[55] H. Shinriki, T. Kisu, and S. Kimura, "Promising storage capacitor structures with thin Ta/sub 2/O/sub 5/ film for low-power high-density DRAMs," *IEEE Transactions on Electron Devices*, vol. 37, 1990.

[56] Y. Gong, W. Zhou, Y. Kou, L. Xu, H. Wu, and W. Zhao, "Heat conductive h-BN/CTPB/epoxy with enhanced dielectric properties for potential high-voltage applications," *High Voltage*, vol. 2, no. 3, pp. 172–178, 2017.

[57] V. D. Mote, Y. Purushotham, and B. N. Dole, "Structural, morphological, physical and dielectric properties of Mn doped ZnO nanocrystals synthesized by sol-gel method," *Materials & Design*, vol. 96, pp. 99–105, 2016.

[58] M. Parvez Ahmad, A. Venkateswara Rao, K. Suresh Babu, and G. Narsinga Rao, "Particle size effect on the dielectric properties of ZnO nanoparticles," *Materials Chemistry and Physics*, vol. 224, pp. 79–84, 2019.

[59] R. V. Mangalaraja, P. Manohar, F. D. Gnanam, and M. Awano, "Electrical and magnetic properties of Ni0.8Zn0.2Fe2O4/silica composite prepared by sol-gel

method," *Journal of Materials Science*, vol. 39, no. 6, pp. 2037–2042, 2004.

[60] R. L. De Sousa e Silva and A. Franco, "Effect of porosity on dielectric properties of ZnO ceramics," *Journal of the European Ceramic Society*, vol. 40, no. 4, pp. 1307–1311, 2020.

[61] D. J. Bergman, "The dielectric constant of a composite material-a problem in classical physics," *Physics Reports*, vol. 43, no. 9, pp. 377–407, 1978.

[62] B. Sareni, L. Krähenbühl, A. Beroual, and C. Brosseau, "Effective dielectric constant of random composite materials," *Journal of Applied Physics*, vol. 81, no. 5, pp. 2375–2383, 1997.

[63] G. A. Mohamed, A. B. Abd El-Moiz, and M. Rashad, "Li-doping effects on the electrical properties of ZnO films prepared by the chemical-bath deposition method," *Physica B: Condensed Matter*, vol. 370, no. 1-4, pp. 158–167, 2005.

[64] D. Huang, Z. Liu, Y. Li, and Y. Liu, "Colossal permittivity and dielectric relaxation of (Li, In) co-doped ZnO ceramics," *Journal of Alloys and Compounds*, vol. 698, pp. 200–206, 2017.

[65] R. Khan, F. Zulfiqar, C. I. Levartoski de Araujo et al., "Influence of oxygen vacancies on the structural, dielectric, and magnetic properties of (Mn, Co) co-doped ZnO nanostructures," *Journal of Materials Science: Materials in Electronics*, vol. 29, no. 12, pp. 9785–9795, 2018.

[66] R. Silva, P. Banerjee, and A. Franco Júnior, "Functional properties of donor- and acceptor-co-doped high dielectric constant zinc oxide ceramics," *Physical Chemistry Chemical Physics*, vol. 21, no. 18, pp. 9456–9464, 2019.

[67] H. Kurnia and E. Suharyadi, "Study on the influence of crystal structure and grain size on dielectric properties of manganese ferrite ($MnFe_2O_4$) nanoparticles," *IOP Conference Series: Materials Science and Engineering*, vol. 202, 2017.

[68] K. M. Lee, C. W. Lai, K. S. Ngai, and J. C. Juan, "Recent developments of zinc oxide based photocatalyst in water treatment technology: a review," *Water Research*, vol. 88, pp. 428–448, 2016.

[69] T. Cun, C. Dong, and Q. Huang, "Ionothermal precipitation of highly dispersive ZnO nanoparticles with improved photocatalytic performance," *Applied Surface Science*, vol. 384, pp. 73–82, 2016.

[70] K. N. Abbas and N. Bidin, "Morphological driven photocatalytic activity of ZnO nanostructures," *Applied Surface Science*, vol. 394, pp. 498–508, 2017.

[71] A. Akyol, H. C. Yatmaz, and M. Bayramoglu, "Photocatalytic decolorization of remazol red RR in aqueous ZnO suspensions," *Applied Catalysis B: Environmental*, vol. 54, pp. 19–24, 2004.

[72] G. Colon, M. C. Hidalgo, J. A. Navío, E. Pulido Melian, O. Gonzalez Díaz, and J. M. Dona Rodríguez, "Highly photoactive ZnO by amine capping-assisted hydrothermal treatment," *Applied Catalysis B: Environmental*, vol. 83, pp. 30–38, 2008.

[73] C. Lizama, J. Freer, J. Baeza, and H. D. Mansilla, "Optimized photodegradation of reactive blue 19 on TiO_2 and ZnO suspensions," *Catalysis Today*, vol. 76, pp. 235–246, 2002.

[74] D. Mijin, M. Savic, P. Snezana et al., "A study of the photocatalytic degradation of metamitron in ZnO water suspensions," *Desalination*, vol. 249, pp. 286–292, 2009.

[75] A. K. Chandiran, M. Abdi-Jalebi, M. K. Nazeeruddin, and M. Grätzel, "Analysis of electron transfer properties of ZnO and TiO2 photoanodes for dye-sensitized solar cells," *ACS Nano*, vol. 8, pp. 2261–2268, 2014.

[76] J. A. Anta, E. Guillen, and R. Tena-Zaera, "ZnO-based dye-sensitized solar cells," *The Journal of Physical Chemistry C*, vol. 116, pp. 11413–11425, 2012.

[77] V. Kandavelu, H. Kastien, and K. R. Thampi, "Photocatalytic degradation of iso- thiazolin-3-ones in water and emulsion paints containing nanocrystalline TiO_2 and ZnO catalysts," *Applied Catalysis B: Environmental*, vol. 48, pp. 101–111, 2004.

[78] M. Mehedi Hassan, A. S. Ahmed, M. Chaman, W. Khan, A. H. Naqvi, and A. Azam, "Structural and frequency dependent dielectric properties of Fe3+ doped ZnO nanoparticles," *Materials Research Bulletin*, vol. 47, no. 12, pp. 3952–3958, 2012.

[79] S. Ambika and M. Sundrarajan, "Antibacterial behaviour of vitex negundo extract assisted ZnO nanoparticles against pathogenic bacteria," *Journal of Photochemistry and Photobiology. B, Biology*, vol. 146, pp. 52–57, 2015.

[80] J. Panigrahi, D. Behera, I. Mohanty, U. Subudhi, B. B. Nayak, and B. S. Acharya, "Radio frequency plasma enhanced chemical vapor based ZnO thin film deposition on glass substrate: a novel approach towards antibacterial agent," *Applied Surface Science*, vol. 258, pp. 304–311, 2011.

[81] P. Zhu, Z. Weng, X. Li et al., "Biomedical applications of functionalized ZnO nanomaterials: from biosensors to bioimaging," *Advanced Materials Interfaces*, vol. 3, no. 1, Article ID 1500494, 2016.

[82] V. Svetlichnyi, A. Shabalina, I. Lapin, D. Goncharova, and A. Nemoykina, "ZnO nanoparticles obtained by pulsed laser ablation and their composite with cotton fabric: preparation and study of antibacterial activity," *Applied Surface Science*, vol. 372, pp. 20–29, 2016.

[83] N. Güy and M. €Ozacar, "The influence of noble metals on photocatalytic activity of ZnO for congo red degradation," *International Journal of Hydrogen Energy*, vol. 41, pp. 20100–20112, 2016.

[84] V. E. Podasca, T. Buruiana, and E. C. Buruiana, "UV-cured polymeric films containing ZnO and silver nanoparticles with UVevis light-assisted photocatalytic ac- tivity," *Applied Surface Science*, vol. 377, pp. 262–273, 2016.

[85] K. Shim, M. Abdellatif, E. Choi, and D. Kim, "Nanostructured ZnO films on stainless steel are highly safe and effective for antimicrobial applications," *Applied Microbiology and Biotechnology*, vol. 7, pp. 2801–2809, 2017.

[86] G. He, E. I. Pearce, and C. H. Sissons, "Inhibitory effect of ZnCl(2) on glycolysis in human oral microbes," *Archives of Oral Biology*, vol. 47, pp. 117–129, 2002.

[87] S. George, S. Pokhrel, T. Xia et al., "Use of a rapid cytotoxicity screening approach to engineer a safer zinc oxide nanoparticle through iron doping," *ACS Nano*, vol. 4, pp. 15–29, 2010.

[88] V. Kononenko, N. Repar, N. Marušič, B. Drašler, T. Romih, and S. Hočevar, D. Drobne, Comparative in vitro genotoxicity study of ZnO nanoparticles, ZnO macroparticles and ZnCl2 to MDCK kidney cells: size matters," *Toxicology in Vitro: An International Journal Published in Association with BIBRA*, vol. 40, pp. 256–263, 2017.

[89] S. Hackenberg, A. Scherzed, A. Technau et al., "Cytotoxic, genotoxic and pro-inflammatory effects of zinc oxide nanoparticles in human nasal mucosa cells in vitro," *Toxicology in Vitro: An International Journal Published in Association with BIBRA*, vol. 25, pp. 657–663, 2011.

[90] C. B. Ong, L. Y. Ng, and A. W. Mohammad, "A review of ZnO nanoparticles as solar photocatalysts: synthesis,

mechanisms and applications," *Renewable and Sustainable Energy Reviews*, vol. 81, pp. 536–551, 2018.

[91] S. Xu and Z. L. Wang, "One-dimensional ZnO nanostructures: solution growth and functional properties," *Nano Research*, vol. 4, no. 11, pp. 1013–1098, 2011.

[92] H. Li, X Zhang, N Liu et al., "Enhanced photo-response properties of a single ZnO microwire photodetector by coupling effect between localized Schottky barriers and piezoelectric potential," *Optics Express*, vol. 23, pp. 21204–21212, 2015.

[93] D. C. Onwudiwe, T. Arfin, and C. A. Strydom, "Surfactant mediated synthesis of ZnO nanospheres at elevated temperature, and their dielectric properties," *Superlattices and Microstructures*, vol. 81, pp. 215–225, 2015.

[94] N. Wiesmann, M. Kluenker, P. Demuth, W. Brenner, W. Tremel, and J. Brieger, "Zinc overload mediated by zinc oxide nanoparticles as innovative anti-tumor agent," *Journal of Trace Elements in Medicine and Biology*, vol. 51, pp. 226–234, 2019.

[95] M. Khatami, R. S. Varma, N. Zafarnia, H. Yaghoobi, M. Sarani, and V. G. Kumar, "Applications of green synthesized Ag, ZnO and Ag/ZnO nanoparticles for making clinical antimicrobial wound-healing bandages," *Sustainable Chemistry and Pharmacy*, vol. 10, pp. 9–15, 2018.

[96] A. Król, P. Pomastowski, K. Rafińska, V. Railean-Plugaru, and B. Buszewski, "Zinc oxide nanoparticles: synthesis, antiseptic activity and toxicity mechanism," *Advances in Colloid and Interface Science*, vol. 249, pp. 37–52, 2017.

[97] J. V. Chandar, S. Shanmugan, D. Mutharasu, and A. A. Aziz, "Dielectric and UV Absorption studies of ZnO nanoparticles reinforced Polyv (3-hydroxybutyrate) biocomposites for UV," *Biopolymer Nanocomposites*, vol. 8, pp. 123–128, 2016.

[98] L. Al-Naamani, S. Dobretsov, and J. Dutta, "Chitosan-zinc oxide nanoparticle composite coating for active food packaging applications," *Innovative Food Science & Emerging Technologies*, vol. 38, pp. 231–237, 2016.

[99] Y. K. Mishra and R. Adelung, "ZnO tetrapod materials for functional applications," *Materials Today*, vol. 21, no. 6, pp. 631–651, 2018.

[100] X. Gu, T. Qiu, W. Zhang, and P. K. Chu, "Light-emitting diodes enhanced by localized surface plasmon resonance," *Nanoscale Research Letters*, vol. 6, no. 1, pp. 199–212, 2011.

[101] P. Uthirakumar, Y.-S. Lee, E.-K. Suh, and C.-H. Hong, "Hybrid fluorescent polymer-zinc oxide nanoparticles: improved efficiency for luminescence conversion LED," *Journal of Luminescence*, vol. 128, no. 3, pp. 287–296, 2008.

[102] A. Kolodziejczak-Radzimska and T. Jesionowski, "Zinc oxide-from synthesis to application: a review," *Materials (Basel)*.vol. 7, pp. 2833–2881, 2014.

[103] J. McKittrick et al., "Phosphor selection considerations for near-UV LED solid state lighting," *ECS Journal of Solid State Science and Technology*, vol. 2, pp. 3119–3131, 2013.

[104] B. Karthikeyan, T. Pandiyarajan, and R. V. Mangalaraja, "Enhanced blue light emission in transparent ZnO:PVA nanocomposite free standing polymer films," *Spectrochimica Acta Part A: Molecular and Biomolecular Spectroscopy*, vol. 152, pp. 485–490, 2016.

[105] F. H. Alshammari, P. K. Nayak, Z. Wang, and H. N. Alshareef, "Enhanced ZnO thin-film transistor performance using bilayer gate dielectrics," *ACS Applied Materials & Interfaces*, vol. 8, no. 35, pp. 22751–22755, 2016.

[106] J.-S. Park, H. Kim, and I.-D. Kim, "Overview of electroceramic materials for oxide semiconductor thin film transistors," *Journal of Electroceramics*, vol. 32, no. 2-3, pp. 117–140, 2014.

[107] S. Lee, H. Kim, D. J. Yun, S. W. Rhee, and K. Yong, "Resistive switching characteristics of ZnO thin film grown on stainless steel for flexible nonvolatile memory devices," *Applied Physics Letters*, vol. 95, pp. 13–16, 2009.

[108] Z. Zang, "Efficiency enhancement of ZnO/Cu_2O solar cells with well oriented and micrometer grain sized Cu_2O films," *Applied Physics Letters*, vol. 112, 2018.

[109] K. Qi, B. Cheng, J. Yu, and W. Ho, "Review on the improvement of the photocatalytic and antibacterial activities of ZnO," *Journal of Alloys and Compounds*, vol. 727, pp. 792–820, 2017.

[110] M. A. Basyooni, M. Shaban, and A. M. El Sayed, "Enhanced gas sensing properties of spin-coated Na-doped ZnO nanostructured films," *Scientific Reports*, vol. 7, pp. 41716–41812, 2017.

[111] C. Li, Z. Zang, C. Han et al., "Highly compact CsPbBr3 perovskite thin films decorated by ZnO nanoparticles for enhanced random lasing," *Nano Energy*, vol. 40, pp. 195–202, 2017.

[112] M. Laurenti, N. Garino, S. Porro, M. Fontana, and C. Gerbaldi, "Zinc oxide nanostructures by chemical vapour deposition as anodes for Li-ion batteries," *Journal of Alloys and Compounds*, vol. 640, pp. 321–326, 2015.

[113] C. Li, C. Han, Y. Zhang et al., "Enhanced photoresponse of self-powered perovskite photodetector based on ZnO nanoparticles decorated CsPbBr3 films," *Solar Energy Materials and Solar Cells*, vol. 172, pp. 341–346, 2017.

[114] S. Adachi, *Handbook on Physical Properties of Semiconductor*, Springer, New York, NY, USA, 2004.

[115] D. C. Look, D. C. Reynolds, J. R. Sizelove et al., "Electrical properties of bulk ZnO," *Solid State Communications*, vol. 105, no. 6, pp. 399–401, 1998.

[116] N. H. Langton and D. Matthews, "The dielectric constant of zinc oxide over a range of frequencies," *British Journal of Applied Physics*, vol. 9, no. 11, pp. 453–456, 1958.

[117] S. Sharma, C. Periasamy, and P. Chakrabarti, "Thickness dependent study of RF sputtered ZnO thin films for optoelectronic device applications," *Electronic Materials Letters*, vol. 11, no. 6, pp. 1093–1101, 2015.

[118] X. D. Li et al., "A study on the evolution of dielectric function of ZnO thin films with decreasing film thickness," *Journal of Applied Physics*, vol. 115, pp. 1–6, 2014.

[119] D. Pal, J. Singhal, A. Mathur et al., "Effect of substrates and thickness on optical properties in atomic layer deposition grown ZnO thin films," *Applied Surface Science*, vol. 421, pp. 341–348, 2017.

[120] M. L. Dinesha, G. D. Prasanna, C. S. Naveen, and H. S. Jayanna, "Structural and dielectric properties of Fe doped ZnO nanoparticles," *Indian Journal of Physics*, vol. 87, no. 2, pp. 147–153, 2013.

[121] M. Mehedi Hassan, W. Khan, A. Azam, and A. H. Naqvi, "Influence of Cr incorporation on structural, dielectric and optical properties of ZnO nanoparticles," *Journal of Industrial and Engineering Chemistry*, vol. 21, pp. 283–291, 2015.

[122] M. N. Siddique, T. Ali, A. Ahmed, and P. Tripathi, "Enhanced electrical and thermal properties of pure and Ni substituted ZnO Nanoparticles," *Nano-Structures & Nano-Objects*, vol. 16, pp. 156–166, 2018.

[123] J. Iqbal, N. Safdar, T. Jan et al., "Facile synthesis as well as structural, Raman, dielectric and antibacterial characteristics of Cu doped ZnO nanoparticles," *Journal of Materials Science & Technology*, vol. 31, no. 3, pp. 300–304, 2015.

[124] S. Suresh, "Studies on the dielectric properties of CdS nanoparticles," *Applied Nanoscience*, vol. 4, no. 3, pp. 325–329, 2014.

[125] T. A. Safeera and E. I. Anila, "Wet chemical synthesis of chitosan capped ZnO:Na nanoparticles for luminescence applications," *International Journal of Biological Macromolecules*, vol. 104, pp. 1833–1836, 2017.

[126] K. Sato and H. Katayama-Yoshida, "Material design for transparent ferromagnets with ZnO-based magnetic semiconductors," *Japanese Journal of Applied Physics*, vol. 39, 2000.

[127] J. Neamtu and M. Volmer, "The influence of doping with transition metal ions on the structure and magnetic properties of zinc oxide thin films," *The Scientific World Journal*, vol. 20147 pages, 2014.

[128] S. Singh, J. N. D. Deepthi, B. Ramachandran, and M. S. R. Rao, "Synthesis and comparative study of Ho and y doped ZnO nanoparticles," *Materials Letters*, vol. 65, no. 19-20, pp. 2930–2933, 2011.

[129] S. Das, S. Das, and S. Sutradhar, "Effect of Gd 3+ and Al 3+ on optical and dielectric properties of ZnO nanoparticle prepared by two-step hydrothermal method," *Ceramics International*, vol. 43, no. 9, pp. 6932–6941, 2017.

[130] A. Franco Jr and H. V. S. Pessoni, "Effect of Gd doping on the structural, optical band-gap, dielectric and magnetic properties of ZnO nanoparticles," *Physica B: Condensed Matter*, vol. 506, pp. 145–151, 2017.

[131] S. A. Ansari, A. Nisar, B. Fatma, W. Khan, and A. H. Naqvi, "Investigation on structural, optical and dielectric properties of Co doped ZnO nanoparticles synthesized by gel-combustion route," *Materials Science and Engineering: B*, vol. 177, no. 5, pp. 428–435, 2012.

[132] A. F. Jr and H. V. S. Pessoni, "Enhanced dielectric constant of Co-doped ZnO nanoparticulate powders," *Physica B: Condensed Matter*, vol. 476, pp. 12–18, 2015.

[133] S. O. Kasap, *Principles of Electronic Materials and Devices*, McGraw Hill Education, New York, NY, USA, 2001.

[134] J. Maxwell, "A treatise on electricity and magnetism," 1873.

[135] C. G. Koops, "On the dispersion of resistivity and dielectric constant of some semiconductors at audiofrequencies," *Physical Review*, vol. 83, no. 1, pp. 121–124, 1951.

[136] K. W. . Wagner, "Zur theorie der unvollkommenen dielektrika," *Annalen der Physik*, vol. 345, no. 5, 1913.

[137] Z. Bin, Z. Shaomin, W. Haiwei, and D. Zuliang, "Raman scattering and photoluminescence of Fe-doped ZnO nanocantilever arrays," *Science Bulletin*, vol. 53, no. 11, pp. 1639–1643, 2008.

[138] H. Liu, J. Yang, Y. Zhang, L. Yang, M. Wei, and X. Ding, "Structure and magnetic properties of Fe-doped ZnO prepared by the sol–gel method," *Condensed Matter*, vol. 10, 2009.

[139] B. Rajesh Kumar, B. Hymavathi, and T. Subba Rao, "Effect of the ceria dopant on the structural and dielectric properties of ZnO semiconductors," *Journal of Science: Advanced Materials and Devices*, vol. 3, no. 4, pp. 433–439, 2018.

[140] S. Goel, N. Sinha, H. Yadav, S. Godara, A. J. Joseph, and B. Kumar, "Ferroelectric Gd-doped ZnO nanostructures: enhanced dielectric, ferroelectric and piezoelectric properties," *Materials Chemistry and Physics*, vol. 202, pp. 56–64, 2017.

[141] S. Goel, N. Sinha, H. Yadav, A. J. Joseph, and B. Kumar, "Experimental investigation on the structural, dielectric, ferroelectric and piezoelectric properties of La doped ZnO nanoparticles and their application in dye-sensitized solar cells," *Physica E: Low-Dimensional Systems and Nanostructures*, vol. 91, pp. 72–81, 2017.

[142] N. K. Divya and P. P. Pradyumnan, "Enhancement of photocatalytic activity in Nd doped ZnO with an increase in dielectric constant," *Journal of Materials Science: Materials in Electronics*, vol. 28, no. 2, pp. 2147–2156, 2017.

[143] A. Franco and H. V. Pessoni, "Optical band-gap and dielectric behavior in Ho -doped ZnO nanoparticles," *Materials Letters*, vol. 180, pp. 305–308, 2016.

[144] R. Zamiri, A. Kaushal, A. Rebelo, and J. M. F. Ferreira, "Er doped ZnO nanoplates: synthesis, optical and dielectric properties," *Ceramics International*, vol. 40, no. 1, pp. 1635–1639, 2014.

[145] A. Bandyopadhyay, N. Bhakta, S. Sutradhar et al., "Microstructure investigation, optical properties and magnetic phase transition of Tm3+ substituted nanocrystalline ZnO (Zn0.95Tm0.05O)," *RSC Advances*, vol. 6, no. 104, pp. 101818–101826, 2016.

[146] T. Tanaka, G. C. Montanari, and R. Mulhaupt, "Polymer nanocomposites as dielectrics and electrical insulation-perspectives for processing technologies," *Material Characterization and Future Applications*, vol. 11, no. 5, 2004.

[147] M. F. Frechette, M. L. Trudeau, H. D. Alamdari, and S. Boily, "Introductory remarks on nanodielectrics," *IEEE Transactions on Dielectrics and Electrical Insulation*, vol. 11, no. 5, pp. 808–818, 2004.

[148] M. Kozako, N. Fuse, Y. Ohki, T. Okamoto, and T. Tanaka, "Surface degradation of polyamide nanocomposites caused by partial discharges using IEC (b) electrodes," *IEEE Transactions on Dielectrics and Electrical Insulation*, vol. 11, no. 5, pp. 833–839, 2004.

[149] W. Peukert, H.-C. Schwarzer, M. Götzinger, L. Günther, and F. Stenger, "Control of particle interfaces - the critical issue in nanoparticle technology," *Advanced Powder Technology*, vol. 14, no. 4, pp. 411–426, 2003.

[150] B. J. Ash, R. W. Siegel, and L. S. Schadler, "Glass-transition temperature behavior of alumina/PMMA nanocomposites," *Journal of Polymer Science Part B: Polymer Physics*, vol. 42, no. 23, pp. 4371–4383, 2004.

[151] B. J. Ash et al., "Mechanical properties of AI , O ,! polymethylmethacrylate nanocomposites," *Polymer Composites*, vol. 23, 2002.

[152] Z.-M. Dang, L.-Z. Fan, S.-J. Zhao, and C.-W. Nan, "Preparation of nanosized ZnO and dielectric properties of composites filled with nanosized ZnO," *Materials Science and Engineering: B*, vol. 99, no. 1-3, pp. 386–389, 2003.

[153] M. Samet, V Levchenko, G Boiteux, G Seytre, A Kallel, and A Serghei, "Electrode polarization vs. Maxwell-Wagner-Sillars interfacial polarization in dielectric spectra of materials: characteristic frequencies and scaling laws," *The Journal of Chemical Physics*, vol. 142, Article ID 194703, 2015.

[154] S. A. Mansour, R. A. Elsad, and M. A. Izzularab, "Dielectric properties enhancement of PVC nanodielectrics based on synthesized ZnO nanoparticles," *Journal of Polymer Research*, vol. 23, 2016.

[155] S. Choudhary, "Structural, optical, dielectric and electrical properties of (PEO-PVP)-ZnO nanocomposites," *Journal of Physics and Chemistry of Solids*, vol. 121, pp. 196–209, 2018.

[156] J. I. Hong, P. Winberg, L. S. Schadler, and R. W. Siegel, "Dielectric properties of zinc oxide/low density polyethylene nanocomposites," *Materials Letters*, vol. 59, no. 4, pp. 473–476, 2005.

[157] A. Mahmood, A. Naeem, A. Mahmood, and A. Naeem, "High- *K* polymer nanocomposites nanocomposites for for

energy energy storage storage applications," *Properties and Applications of Polymer Dielectrics*, vol. 90, 2017.

[158] C.-C. Shih, W.-Y. Lee, Y.-C. Chiu et al., "High performance transparent transistor memory devices using nano-floating gate of polymer/ZnO nanocomposites," *Scientific Reports*, vol. 6, no. 1, p. 10, 2016.

[159] Z. A. Kösemen, A. Kösemen, S. Öztürk et al., "Effect of intrinsic polymer properties on the photo sensitive organic field-effect transistors (Photo-OFETs)," *Microelectronic Engineering*, vol. 161, pp. 36–42, 2016.

[160] S. Bi, Y. Li, Z. He, Z. Ouyang, Q. Guo, and C. Jiang, "Self-assembly diketopyrrolopyrrole-based materials and polymer blend with enhanced crystal alignment and property for organic field-effect transistors," *Organic Electronics*, vol. 65, pp. 96–99, 2019.

[161] B. B. Patowary, S. Laskar, P. P. Sahu, and R. Narzary, "Fabrication and electrical characterization of organic field-effect transistor based on CSA doped PANi-Ta 2 O 5 nanocomposite," *ADBU Journal of Engineering Technology (AJET)*, vol. 9, pp. 1–8, 2020.

[162] S. Cichosz, A. Masek, and M. Zaborski, "Polymer-based sensors: a review," *Polymer Testing*, vol. 67, pp. 342–348, 2018.

[163] Z. Xiao, L. B. Kong, S. Ruan et al., "Recent development in nanocarbon materials for gas sensor applications," *Sensors and Actuators B: Chemical*, vol. 274, pp. 235–267, 2018.

[164] R. Megha, F. A. Ali, Y. T. Ravikiran et al., "Conducting polymer nanocomposite based temperature sensors: a review," *Inorganic Chemistry Communications*, vol. 98, pp. 11–28, 2018.

[165] A. Jafari and A. Amini, "Lactic acid gas sensor based on polypyrrole thin film," *Materials Letters*, vol. 236, pp. 175–178, 2019.

[166] A. Husain, M. U. Shariq, and F. Mohammad, "DC electrical conductivity and liquefied petroleum gas sensing application of polythiophene/zinc oxide nanocomposite," *Materialia*, vol. 9, Article ID 100599, 2020.

[167] L. Lan, P. Cai, Y. Mai et al., "A new wide-bandgap conjugated polymer based on imide-fused benzotriazole for highly efficient nonfullerene polymer solar cells," *Dyes and Pigments*, vol. 158, pp. 219–224, 2018.

[168] F. Arabpour Roghabadi, N. Ahmadi, V. Ahmadi et al., "Bulk heterojunction polymer solar cell and perovskite solar cell: concepts, materials, current status, and opto-electronic properties," *Solar Energy*, vol. 173, pp. 407–424, 2018.

[169] G. Li et al., "A new narrow bandgap polymer as donor material for high performance non- fullerene polymer solar cells," *Organic Electronics*, vol. 64, pp. 241–246, 2018.

[170] G. Sai-Anand, A. Dubey, A.-I. Gopalan et al., "Additive assisted morphological optimization of photoactive layer in polymer solar cells," *Solar Energy Materials and Solar Cells*, vol. 182, pp. 246–254, 2018.

[171] M. Naskar, H. M. Dharmendra, and G. L. Sarode, "Preparation and properties of nano zinc oxide doped ethylene vinyl acetate nanocomposites for solar cell encapsulation," *Materials Today: Proceedings*, vol. 27, pp. 1939–1942, 2019.

[172] M. Yoke, "Enhancing the performance of green solid-state electric double-layer capacitor incorporated with fumed silica nanoparticles," *Journal of Physics and Chemistry of Solids*, vol. 117, pp. 194–203, 2018.

[173] Z. Pan, L. Yao, J. Zhai, X. Yao, and H. Chen, "Interfacial coupling effect in organic/inorganic nanocomposites with high energy density," *Advanced Materials*, vol. 2, pp. 1–7, 2018.

[174] D. Zhang, Z. Wu, X.-f. Zhou, A.-q. Wei, C. Chen, and H. Luo, "High energy density in P(VDF-HFP) nanocomposite with paraffin engineered BaTiO3 nanoparticles," *Sensors and Actuators A: Physical*, vol. 260, pp. 228–235, 2017.

[175] J. Chen, X. Wang, X. Yu et al., "High dielectric constant and low dielectric loss poly(vinylidene fluoride) nanocomposites via a small loading of two-dimensional $Bi_2Te_3@Al_2O_3$ hexagonal nanoplates," *Journal of Materials Chemistry C*, vol. 6, no. 2, pp. 271–279, 2018.

[176] P. Arunachalam, "Polymer-based nanocomposites for energy and environmental applications," *Polymer-based Nanocomposites for Energy and Environmental Applications*, vol. 30, pp. 185–203, 2018.

[177] S. Chakraborty, M. Amla, and A. R. Mary, "Biocompatible supercapacitor electrodes using green synthesised ZnO/Polymer nanocomposites for efficient energy storage applications," *Journal of Energy Storage*, vol. 28, Article ID 101275, 2020.

[178] A. Shayesteh Zeraati and U. Sundararaj, "Carbon nanotube/ZnO nanowire/polyvinylidene fluoride hybrid nanocomposites for enhanced electromagnetic interference shielding," *The Canadian Journal of Chemical Engineering*, vol. 98, no. 5, pp. 1036–1046, 2020.

[179] S. Zhang, G. Sun, Y. He, R. Fu, Y. Gu, and S. Chen, "Preparation, characterization, and electrochromic properties of nanocellulose-based polyaniline nanocomposite films," *ACS Applied Materials & Interfaces*, vol. 9, no. 19, pp. 16426–16434, 2017.

[180] F. Xu, H. Zhang, L. Jin et al., "Controllably degradable transient electronic antennas based on water-soluble PVA/TiO_2 films," *Journal of Materials Science*, vol. 53, no. 4, pp. 2638–2647, 2018.

[181] M. Belhaj, C. Dridi, H. Elhouichet, and J. C. Valmalette, "Study of ZnO nanoparticles based hybrid nanocomposites for optoelectronic applications," *Journal of Applied Physics*, vol. 119, 2016.

[182] H. Zhang, X. Zhao, J. Huang et al., "Bistable non-volatile resistive memory devices based on ZnO nanoparticles embedded in polyvinylpyrrolidone," *RSC Advances*, vol. 10, no. 25, pp. 14662–14669, 2020.

[183] E. Helal, C. Pottier, E. David, M. Fréchette, and N. R. Demarquette, "Polyethylene/thermoplastic elastomer/Zinc Oxide nanocomposites for high voltage insulation applications: dielectric, mechanical and rheological behavior," *European Polymer Journal*, vol. 100, pp. 258–269, 2018.

[184] D. Ponnamma, J.-J. Cabibihan, M. Rajan et al., "Synthesis, optimization and applications of ZnO/polymer nanocomposites," *Materials Science and Engineering: C*, vol. 98, pp. 1210–1240, 2019.

[185] J. Anandraj and G. M. Joshi, "Fabrication, performance and applications of integrated nanodielectric properties of materials - a review," *Composite Interfaces*, vol. 25, no. 5-7, pp. 455–489, 2018.

[186] S. Choudhary, "Characterization of amorphous silica nanofiller effect on the structural, morphological, optical, thermal, dielectric and electrical properties of PVA-PVP blend based polymer nanocomposites for their flexible nanodielectric applications," *Journal of Materials Science: Materials in Electronics*, vol. 29, no. 12, pp. 10517–10534, 2018.

[187] A. Geczy, T. Garami, B. Kovacs et al., "Soldering tests with biodegradable printed circuit boards," in *Proceedings of the 2013 IEEE 19th International Symposium for Design and*

Technology in Electronic Packaging (SIITME), pp. 39–42, Galati, Romania, October 2013.

[188] A. Geczy, M. Kovacs, and I. Hajdu, "Conductive layer deposition and peel tests on biodegradable printed circuit boards," in *Proceedings of the 2012 IEEE 18th International Symposium for Design and Technology in Electronic Packaging (SIITME)*, pp. 139–142, Alba Iulia, Romania, October 2012.

[189] P. Nayak, S. Kumar, I. Sinha, and K. K. Singh, "ZnO/CuO nanocomposites from recycled printed circuit board: preparation and photocatalytic properties," *Environmental Science and Pollution Research*, vol. 26, no. 16, pp. 16279–16288, 2019.

[190] V. C. Janakiraman, S. Subramani, M. Devarajan, and A. Abdul Aziz, "Impact of ZnO nanoparticles on dielectric and optical properties of poly (3-hydroxybutyrate) for electronics applications," *Polymer-Plastics Technology and Engineering*, vol. 56, no. 14, pp. 1495–1504, 2017.

[191] A. Bashir, S. Jabeen, N. Gull et al., "Co-concentration effect of silane with natural extract on biodegradable polymeric films for food packaging," *International Journal of Biological Macromolecules*, vol. 106, pp. 351–359, 2018.

[192] Y. Zhong, P. Godwin, Y. Jin, and H. Xiao, "Biodegradable polymers and green-based antimicrobial packaging materials: a mini-review," *Advanced Industrial and Engineering Polymer Research*, vol. 3, no. 1, pp. 27–35, 2020.

[193] M. Ramesh, G. Narendra, and S. Sasikanth, *A Review on Biodegradable Packaging Materials in Extending the Shelf Life and Quality of Fresh Fruits and Vegetables .Waste Management As Economic Industry towards Circular Economy*, Springer, Singapore, Singapore, 2020.

[194] S. K. Fanourakis, J. Peña-Bahamonde, P. C. Bandara, and D. F. Rodrigues, "Nano-based adsorbent and photocatalyst use for pharmaceutical contaminant removal during indirect potable water reuse," *Npj Clean Water*, vol. 3, 2020.

[195] R. Mukhopadhyay, D. Bhaduri, B. Sarkar et al., "Clay-polymer nanocomposites: progress and challenges for use in sustainable water treatment," *Journal of Hazardous Materials*, vol. 383, Article ID 121125, 2020.

[196] J. Karlsson, H. J. Vaughan, and J. J. Green, "Biodegradable polymeric nanoparticles for therapeutic cancer treatments," *Annual Review of Chemical and Biomolecular Engineering*, vol. 9, no. 1, pp. 105–127, 2018.

[197] X. Montané et al., "Encapsulation for cancer therapy," *Molecules*, vol. 25, pp. 1–25, 2020.

[198] M. Alsehli, "Polymeric nanocarriers as stimuli-responsive systems for targeted tumor (cancer) therapy: recent advances in drug delivery," *Saudi Pharmaceutical Journal*, vol. 28, no. 3, pp. 255–265, 2020.

[199] P. Sharma, P. Negi, and N. Mahindroo, "Recent advances in polymeric drug delivery carrier systems," *Advanced Polymer Biomedical Applications*, vol. 10, pp. 369–388, 2018.

[200] E. Calzoni, A Cesaretti, A Polchi, A Di Michele, B Tancini, and C Emiliani, "Biocompatible polymer nanoparticles for drug delivery applications in cancer and neurodegenerative disorder therapies," *Journal of Functional Biomaterials*, vol. 10, no. 1, pp. 1–15, 2019.

[201] W. Mu, Q. Chu, Y. Liu, and N. Zhang, "A review on nano-based drug delivery system for cancer chemo-immunotherapy," *Nano-Micro Letter*, vol. 12, 2020.

[202] R. Ghosh, M. Malhotra, R. R. M. Sathe, and M. Jayakannan, "Biodegradable polymer theranostic fluorescent nanoprobe for direct visualization and quantitative determination of antimicrobial activity," *Biomacromolecules*, vol. 21, no. 7, pp. 2896–2912, 2020.

[203] J. A. Da Cruz, A. B. da Silva, B. B. S. Ramin et al., "Poly(vinyl alcohol)/cationic tannin blend films with antioxidant and antimicrobial activities," *Materials Science and Engineering: C*, vol. 107, Article ID 110357, 2020.

[204] X. Peng, K Dong, C Ye et al., "A breathable, biodegradable, antibacterial, and self-powered electronic skin based on all-nanofiber triboelectric nanogenerators," *Science Advances*, vol. 6, p. 9624, 2020.

[205] M. Silva, F. N. Ferreira, N. M. Alves, and M. C. Paiva, "Biodegradable polymer nanocomposites for ligament/tendon tissue engineering," *Journal of Nanobiotechnology*, vol. 18, pp. 23–33, 2020.

[206] M. Milkoreit, "Wireless implantable and biodegradable sensors for postsurgery monitoring: current status and future perspectives Ac ce pte d M us pt," *Geophysical Research Letters*, vol. 99, pp. 10–31. in Press, 2017.

[207] G. Yang, J. Zhao, S. Yi, X. Wan, and J. Tang, "Biodegradable and photostable Nb2C MXene quantum dots as promising nanofluorophores for metal ions sensing and fluorescence imaging," *Sensors and Actuators B: Chemical*, vol. 309, Article ID 127735, 2020.

[208] A. Sukan, I. Roy, and T. Keshavarz, "Agro-industrial waste materials as substrates for the production of poly(3-hydroxybutyric acid)," *Journal of Biomaterials and Nanobiotechnology*, vol. 5, no. 4, pp. 229–240, 2014.

[209] Ł. Kaniuk, Z. J. Krysiak, S. Metwally, and U. Stachewicz, "Osteoblasts and fibroblasts attachment to poly(3-hydroxybutyric acid-co-3-hydrovaleric acid) (PHBV) film and electrospun scaffolds," *Materials Science & Engineering. C, Materials for Biological Applications*, vol. 110, Article ID 110668, 2020.

[210] H. Brandl, R. A. Gross, R. W. Lenz, and R. C. Fuller, "Plastics from bacteria and for bacteria: poly(beta-hydroxyalkanoates) as natural, biocompatible, and biodegradable polyesters," *Advances in Biochemical Engineering/biotechnology*, vol. 41, pp. 77–93, 1990.

[211] A. Steinbüchel, "Polyhydroxyalkanoic acids," *Biomaterials*, vol. 40, pp. 123–213, 1991.

[212] D. Jendrossek, A. Schirmer, and H. G. Schlegel, "Biodegradation of polyhydroxyalkanoic acids," *Applied Microbiology and Biotechnology*, vol. 46, no. 5-6, pp. 451–463, 1996.

[213] N. Stephen, Lighting and UV radiation: where do LEDs fit in? http://www.leapfroglighting.com/lighting_and_uv_radiation/, 2012.

[214] A. Becheri, M. Dürr, P. Lo Nostro, and P. Baglioni, "Synthesis and characterization of zinc oxide nanoparticles: application to textiles as UV-absorbers," *Journal of Nanoparticle Research*, vol. 10, no. 4, pp. 679–689, 2008.

[215] R. Wang, J. H. Xin, X. M. Tao, and W. A. Daoud, "ZnO nanorods grown on cotton fabrics at low temperature," *Chemical Physics Letters*, vol. 398, no. 1-3, pp. 250–255, 2004.

[216] I. Shahid-Ul, M. Shahid, and F. Mohammad, "Green chemistry approaches to develop antimicrobial textiles based on sustainable biopolymers-a review," *Industrial & Engineering Chemistry Research*, vol. 52, no. 15, pp. 5245–5260, 2013.

[217] C. Shuai et al., "Enhanced crystallinity and antibacterial of PHBV scaffolds incorporated with zinc oxide," *Journal of Nanomaterials*, vol. 2020, Article ID 6014816, 12 pages, 2020.

[218] J. L. Castro-Mayorga, M. J. Fabra, A. M. Pourrahimi, R. T. Olsson, and J. M. Lagaron, "The impact of zinc oxide particle morphology as an antimicrobial and when

incorporated in poly(3-hydroxybutyrate-co-3-hydroxyvalerate) films for food packaging and food contact surfaces applications," *Food and Bioproducts Processing*, vol. 101, pp. 32–44, 2017.

[219] K. J. Figueroa-Lopez, "lectrospun active biopapers of food waste derived poly (3- hydroxybutyrate-co-3-hydroxyvalerate) with short-term and long-term antimicrobial performance," *Nanomaterials*, vol. 10, pp. 1–26, 2020.

[220] M. Zare, K. Namratha, S. Ilyas, A. Hezam, S. Mathur, and K. Byrappa, "Smart fortified PHBV-CS biopolymer with ZnO-Ag nanocomposites for enhanced shelf life of food packaging," *ACS Applied Materials & Interfaces*, vol. 11, no. 51, pp. 48309–48320, 2019.

[221] R. Tarrahi, Z. Fathi, M. Ö. Seydibeyoğlu, E. Doustkhah, and A. Khataee, "Polyhydroxyalkanoates (PHA): from production to nanoarchitecture," *International Journal of Biological Macromolecules*, vol. 146, pp. 596–619, 2020.

[222] S. Kashi, R. K. Gupta, T. Baum, N. Kao, and S. N. Bhattacharya, "Dielectric properties and electromagnetic interference shielding effectiveness of graphene-based biodegradable nanocomposites," *Materials & Design*, vol. 109, pp. 68–78, 2016.

[223] S. Kashi, R. K. Gupta, S. N. Bhattacharya, and R. J. Varley, "Experimental and simulation study of effect of thickness on performance of (butylene adipate-co-terephthalate) and poly lactide nanocomposites incorporated with graphene as stand-alone electromagnetic interference shielding and metal-backed microwave absorbers," *Composites Science and Technology*, vol. 195, Article ID 108186, 2020.

[224] R. Sharma, S. M. Jafari, and S. Sharma, "Antimicrobial bionanocomposites and their potential applications in food packaging," *Food Control*, vol. 112, Article ID 107086, 2020.

[225] P. Mujeeb Rahman, V. M. Abdul Mujeeb, K. Muraleedharan, and S. K. Thomas, "Chitosan/nano ZnO composite films: enhanced mechanical, antimicrobial and dielectric properties," *Arabian Journal of Chemistry*, vol. 11, no. 1, pp. 120–127, 2018.

[226] S. Yadav, G. K. Mehrotra, and P. K. Dutta, "Chitosan based ZnO nanoparticles loaded gallic-acid films for active food packaging," *Food Chemistry*, vol. 334, Article ID 127605, 2021.

[227] S. Kumar, A. Mudai, B. Roy, I. B. Basumatary, A. Mukherjee, and J. Dutta, "Biodegradable hybrid nanocomposite of chitosan/gelatin and green synthesized zinc oxide nanoparticles for food packaging," *Foods*, vol. 9, no. 9, p. 1143, 2020.

[228] K. Pandiselvi and S. Thambidurai, "Chitosan-ZnO/polyaniline ternary nanocomposite for high-performance supercapacitor," *Ionics*, vol. 20, no. 4, pp. 551–561, 2014.

[229] H. El Knidri, R. Belaabed, A. Addaou, A. Laajeb, and A. Lahsini, "Extraction, chemical modification and characterization of chitin and chitosan," *International Journal of Biological Macromolecules*, vol. 120, pp. 1181–1189, 2018.

[230] O. Boura-Theodoridou, A. Giannakas, P. Katapodis, H. Stamatis, A. Ladavos, and N.-M. Barkoula, "Performance of ZnO/chitosan nanocomposite films for antimicrobial packaging applications as a function of NaOH treatment and glycerol/PVOH blending," *Food Packaging and Shelf Life*, vol. 23, Article ID 100456, 2020.

[231] R. Zhong, Q. Zhong, M. Huo, B. Yang, and H. Li, "Preparation of biocompatible nano-ZnO/chitosan microspheres with multi-functions of antibacterial, UV-shielding and dye photodegradation," *International Journal of Biological Macromolecules*, vol. 146, pp. 939–945, 2020.

[232] S. Kumar, B. Krishnakumar, A. J. F. N. Sobral, and J. Koh, "Bio-based (chitosan/PVA/ZnO) nanocomposites film: thermally stable and photoluminescence material for removal of organic dye," *Carbohydrate Polymers*, vol. 205, pp. 559–564, 2019.

[233] S.-B. Ghaffari, M.-H. Sarrafzadeh, M. Salami, and M. R. Khorramizadeh, "A pH-sensitive delivery system based on N-succinyl chitosan-ZnO nanoparticles for improving antibacterial and anticancer activities of curcumin," *International Journal of Biological Macromolecules*, vol. 151, pp. 428–440, 2020.

Hindawi
International Journal of Optics
Volume 2021, Article ID 8897928, 8 pages
https://doi.org/10.1155/2021/8897928

Research Article

Spectral Efficient Asymmetrically Clipped Hybrid FBMC for Visible Light Communication

Sanjeev Kumar and Preeti Singh

Department. of ECE, UIET, Panjab University, Chandigarh, India

Correspondence should be addressed to Preeti Singh; preeti_singh@pu.ac.in

Received 10 September 2020; Revised 3 January 2021; Accepted 9 January 2021; Published 23 January 2021

Academic Editor: Sulaiman W. Harun

Filter bank multicarrier (FBMC) modulation has shown sufficient potential for wireless communication. A hybrid optical FBMC technique is proposed to improve the spectral efficiency of a visible light communication (VLC) system. In this technique, a hybrid asymmetrically clipped optical offset quadrature amplitude modulation FBMC (HACO-OQAM-FBMC) modulation technique is used. Asymmetrically clipped optical FBMC (ACO-FBMC) is used for odd subcarriers, and pulse amplitude modulation-discrete multitone (PAM-DMT) is used for the even subcarriers. The proposed hybrid scheme uses an intensity modulation/direct detection (IM/DD) channel. It is shown that there is no interference on odd subcarriers using the proposed method and receiver demodulation is similar to that of ACO-FBMC receiver. However, clipping noise of ACO-FBMC falls on PAM-DMT subcarriers, which can be cancelled at receiver processing after estimation. The analytical performance of the proposed technique is compared using parameters, namely, bit error rate (BER), spectral efficiency, computational complexity, and peak to average power ratio (PAPR). It is found that HACO-OQAM-FBMC is more spectral efficient than ACO-FBMC and other OFDM-based techniques.

1. Introduction

Orthogonal frequency division multiplexing (OFDM) is used extensively in wired and wireless communication systems. Despite its popularity, it possesses some limitations also such as high out-of-band distortion and long cyclic prefix (CP). In previous years, alternative multicarrier modulation techniques have been studied to address OFDM issues. The filter bank multicarrier (FBMC) modulation technique is considered one of the most potential waveforms for next-generation wireless communications due to its robustness against intersymbol interference (ISI) [1].

Visible light communication (VLC) has drawn great attention of researchers due to its unlicensed spectrum, no health hazards, and no electromagnetic interference [2]. In radio frequency (RF) communications, FBMC has been considered as a strong competitor of OFDM [3, 4]. But, for the VLC system, which uses an intensity modulation/direct detection (IM/DD) channel, the signal should be real and unipolar [5–7]. Moreover, the average power of RF communication is the mean square value of the signal, but the average power of VLC is the mean value of the signal. A lower average power is usually preferred for RF communication, but VLC has a predefined average intensity according to the dimming target, which is not an objective function but a constraint [8, 9]. So, FBMC techniques as implemented in RF communications straightforward cannot be used in the VLC system.

The modulation techniques mostly used in the VLC system are asymmetrical clipped optical OFDM (ACO-OFDM) and DC biased optical OFDM (DCO-OFDM). Spectral efficiency of ACO-OFDM is low because only odd subcarriers are used and even subcarriers are neglected to meet the requirement of the VLC system [10]. To improve the spectral efficiency of the VLC system mostly proposed techniques in literature are based on OFDM. Asymmetrically clipped DC biased OFDM (ADO-OFDM) to improve the spectral efficiency of ACO-OFDM is proposed in [11]. But, it uses DC bias for even subcarriers which is a power inefficient method. In [12], the author proposed enhanced hybrid asymmetrically clipped OFDM (EHACO-OFDM) which increases spectral efficiency but has more complexity.

Till date, there is no work reported in the literature which discusses the assessment of the hybrid FBMC modulation technique for VLC based on the IM/DD channel.

In this paper, the authors proposed hybrid asymmetrically clipped optical offset quadrature amplitude modulation FBMC (HACO-OQAM-FBMC) in which ACO-FBMC is used for the odd subcarriers and PAM-DMT is used for the even subcarriers. The clipping noise of ACO-FBMC falls only on even subcarriers. The receiver of HACO-OQAM-FBMC consists of four signals: the wanted ACO-FBMC signal, clipping noise from ACO-FBMC, PAM-DMT signal, and noise added in the channel. The clipping noise of ACO-FBMC can be accurately separated from PAM-DMT after estimation before demodulation.

The authors' contributions can be summarized as follows:

(1) The system model is proposed for the HACO-OQAM-FBMC modulation technique

(2) Scaling techniques are used for the proposed FBMC-based model for the VLC system

(3) The performance analysis is carried out using spectral efficiency, bit error rate (BER), computational complexity, and peak to average power ratio (PAPR) for the FBMC-based VLC system

(4) Non-DC bias methods are used for the proposed model of the VLC system

(5) The performance of ACO-OFDM, DCO-OFDM, ADO-OFDM, EHACO-OFDM, ACO-FBMC, DCO-FBMC, and HACO-OQAM-FBMC modulation techniques has been compared

The content of this paper is systematized as follows. Section 2 gives the system model for the HACO-OQAM-FBMC modulation technique. Performance analysis of the proposed system models is performed in Section 3 using parameters, probability density function, bit error probability, peak to average power ratio, computational complexity, spectral efficiency, and power spectral density. The conclusion is presented in Section 4.

2. Proposed Modulation Techniques System Model

The system model consists of a transmitter and receiver functional diagram for the VLC system. Figure 1 shows the functional diagram of the transmitter and receiver section of the HACO-OQAM-FBMC modulation technique.

In the transmitter section of HACO-OQAM-FBMC, the offset quadrature amplitude modulation (OQAM) is used for signal mapping. Hermitian symmetry is used to fit the signal into VLC system requirements. Odd subcarriers are modulated using an ACO-FBMC modulator, and a PAM-DMT modulator is used for even subcarriers. An optical modulator is employed to convert an electrical signal to optical signal. In the receiver section of HACO-OQAM-FBMC, an optical demodulator is used to convert an optical signal back to an electrical signal. For extraction of even and odd subcarriers, ACO-FBMC and PAM-DMT demodulators are used. The equalizer is used to remove the distortion, and finally, the signal is extracted using a decoder. The signal analysis of the HACO-OQAM-FBMC transmitter and receiver is given in the next section.

2.1. Signal Analysis of the HACO-OQAM-FBMC Transmitter. The data subcarriers are given by $Z = [Z_0, Z_1, Z_2, \ldots, Z_{N-1}]$. The ACO-FBMC consists of odd subcarriers Z_{odd}, and PAM-DMT consists of even subcarriers Z_{even}. The even and odd subcarriers are sent to the PAM-DMT and ACO-FBMC modulators which consist of IFFT and clipping of the signal. The transmitted ACO-FBMC signal is represented by

$$z_{\text{ACO-FBMC}} = z_{\text{odd}} + n_{\text{afcn}}. \tag{1}$$

Similarly, the transmitted signal of PAM-DMT is given by

$$z_{\text{PAM-DMT}} = z_{\text{even}}, \tag{2}$$

where n_{afcn} and n_{dfcn} are the clipping noise of ACO-FBMC and PAM-DMT [13]. Using equations (1) and (2), the transmitted signal of HACO-OQAM-FBMC is given by

$$\begin{aligned} z(t) &= z_{\text{ACO-FBMC}} + z_{\text{PAM-DMT}}, \\ Z(t) &= z_{\text{odd}} + n_{\text{afcn}} + z_{\text{even}}. \end{aligned} \tag{3}$$

Upper-case letters are used to represent frequency-domain signals, and lower-case letters are used to represent time-domain signals.

2.1.1. ACO-FBMC Modulator. The OQAM modulator output shown in Figure 1 consists of a real and imaginary signal. Upsampling is performed before prototype filter to increase the sampling rate. A PHYDYAS protype filter is used in the proposed method. After IFFT execution, clipping is required to fulfil optical modulator constraints. The block diagram of the ACO-FBMC modulator is shown in Figure 2.

The PHYDYAS prototype filter [14] is given by

$$p(t) = \begin{cases} \dfrac{1 + 2\sum_{i=1}^{O-1} c_i \cos\left(2\pi t/\mathrm{KT}_0\right)}{K\sqrt{T_0}/0}, & \text{if } -\dfrac{\mathrm{KT}_0}{2} < t \le \dfrac{\mathrm{KT}_0}{2}. \end{cases} \tag{4}$$

The coefficients c_i depend on the overlapping factor K, and the procedure for calculation is given in [15]. For example, when the value of the overlapping factor $K = 4$, the coefficients are given by

$$\begin{aligned} c_1 &= 1.412692577, \\ c_2 &= 1.41421356237/2, \\ c &= 0.23514695. \end{aligned} \tag{5}$$

Orthogonal: $T = T_0; F = 2/T_0 \longrightarrow \mathrm{TF} = 2$. Localization: $\sigma_t = 0.2015\,T_0$; $\sigma_f = 0.403\,T_0^{-1}$. Joint Localization: $\sigma_t\sigma_f = 1.13 \times (1/4\pi)$.

2.2. Signal Analysis of the HACO-OQAM-FBMC Receiver. The received signal for HACO-OQAM-FBMC is given by

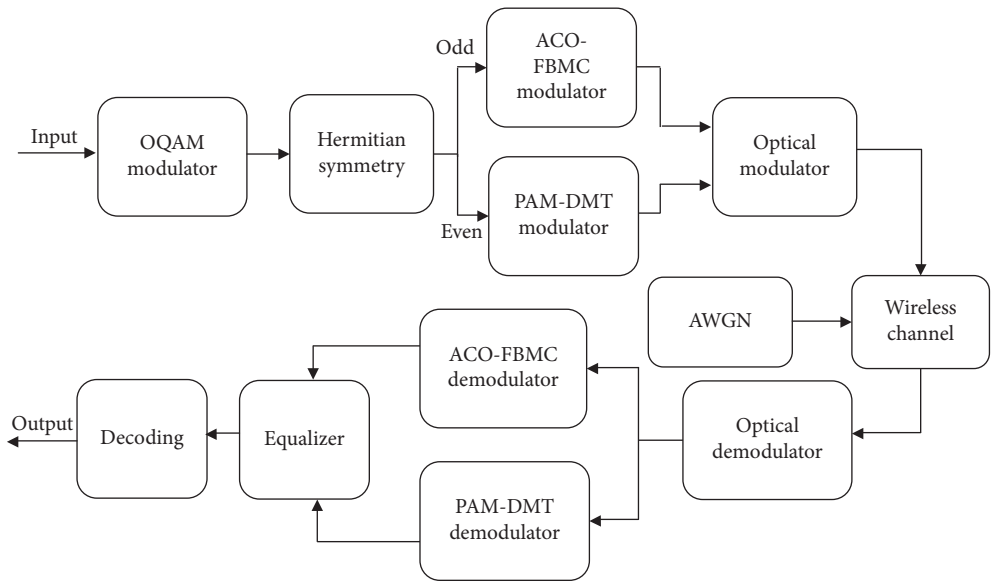

Figure 1: Block diagram of HACO-OQAM-FBMC.

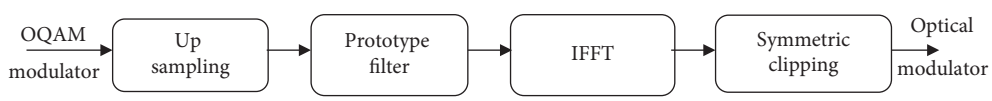

Figure 2: Block diagram of the ACO-FBMC modulator.

$$y(t) = z_{\text{odd}} + n_{\text{afcn}} + z_{\text{even}} + n_{d_{\text{awgn}}} + n_{a_{\text{awgn}}}, \tag{6}$$

where n_{d_awgn} and n_{a_awgn} are the additive white Gaussian noise (AWGN) of the even and odd subcarriers. A flat channel is assumed for one receiver. After applying FFT to equation (6), the signal is given by

$$Y(t) = Z_{\text{odd}} + N_{\text{afcn}} + Z_{\text{even}} + N_{d_{\text{awgn}}} + N_{a_{\text{awgn}}}. \tag{7}$$

The clipping noise and AWGN noise are removed using ACO-FBMC and PAM-DMT demodulators. The decoded signal is given by

$$Y(t) = z_{\text{odd}} + z_{\text{even}}. \tag{8}$$

2.2.1. ACO-FBMC and PAM-DMT Signal Detection. The optical demodulator output, as shown in Figure 1, consist of ACO-FBMC, PAM-DMT, AWGN noise, and clipping noise. The received signal from optical demodulator is converted into frequency domain using FFT. After that, the ACO-FBMC signal is detected. To recover the PAM-DMT signal, we have to use the clipping noise estimation technique, as shown in Figure 3. In this technique, for proper detection and scaling, odd subcarriers are multiplied by 2 because power of the M-QAM symbols reduced by half due to clipping operation [16, 17]. Subtraction of estimated clipping noise which falls on PAM-DMT (even) subcarriers from received ACO-FBMC symbols will give PAM-DMT symbols.

3. Performance Analysis of HACO-OQAM-FBMC

The performance analysis is carried out using probability density function, bit error rate, spectral efficiency, computational complexity, peak to average power ratio, and power spectral density.

3.1. Probability Density Function (PDF) of HACO-OQAM-FBMC. The PDF of HACO-OQAM-FBMC can be calculated by convolving the PDF of ACO-FBMC and PDF of PAM-DMT. The PDF of ACO-FBMC is given by [18, 19]

$$f_{z_{\text{ACO-FBMC}}}(\alpha) = \frac{1}{\sigma\sqrt{2\pi}} \exp\left(\frac{-\alpha^2}{2\sigma_1^2}\right) g(\alpha) + \frac{1}{2}\delta(\alpha). \tag{9}$$

The PDF of PAM-DMT given by [18, 20]

$$f_{z_{\text{PAM-DMT}}}(\beta) = \frac{1}{\sigma\sqrt{2\pi}} \exp\left(\frac{-\beta^2}{2\sigma_2^2}\right) g(\beta) + \frac{1}{2}\delta(\beta). \tag{10}$$

The PDF of HACO-OQAM-FBMC can be calculated using convolution of equations (9) and (10).

$$f_{z_{\text{HACO-FBMC}}}(\gamma) = \int_{-\infty}^{\infty} f_{z_{\text{PAM-DMT}}}(\gamma - \tau) f_{z_{\text{ACO-FBMC}}(t)}(\tau) d\tau. \tag{11}$$

Substituting equations (9) and (10) in equation (11) gives

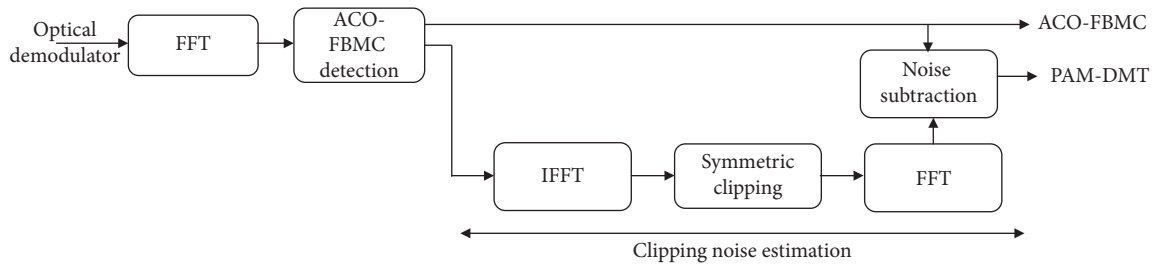

Figure 3: Block diagram of ACO-FBMC and PAM-DMT detection.

$$f_{z_{\text{HACO-OQAM-FBMC}}}(\gamma) = \int_{-\infty}^{\infty}\left(\frac{1}{\sigma\sqrt{2\pi}}\exp\left(\frac{-(\gamma-\tau)^2}{2\sigma_2^2}\right)g(\delta-\tau)+\frac{1}{2}\gamma(\delta-\tau)\right)\times\left(\frac{1}{\sigma\sqrt{2\pi}}\exp\left(\frac{-\tau^2}{2\sigma_1^2}\right)g(\delta-\tau)+\frac{1}{2}\gamma(\delta-\tau)\right)d\tau, \tag{12}$$

where σ^2 is the variance of the signal and is given by $E\{z^2\}$. Using identity [21, 22],

$$\begin{aligned} f_{z_{\text{HACO-OQAM-FBMC}}}(\gamma) = {} & \frac{\exp\left(-z^2/2\sigma_2^2\right)}{\pi\sigma_1\sigma_2}\sqrt{\pi\left(\frac{\sigma_1^2\sigma_2^2}{2\left(\sigma_1^2+\sigma_2^2\right)}\right)}\exp\left(\frac{\gamma^2}{\sigma_2^4}\left(\frac{\sigma_1^2\sigma_2^2}{2\left(\sigma_1^2+\sigma_2^2\right)}\right)\right) \\ & \cdot\left[Q\left(-\frac{\gamma}{\sigma_2^2}\sqrt{2\left(\frac{\sigma_1^2\sigma_2^2}{2\left(\sigma_1^2+\sigma_2^2\right)}\right)}\right)-Q\left(-\frac{\gamma}{\sigma_2^2}\sqrt{2\left(\frac{\sigma_1^2\sigma_2^2}{2\left(\sigma_1^2+\sigma_2^2\right)}\right)}+\frac{\gamma}{\sqrt{2\left(\sigma_1^2\sigma_2^2/2\left(\sigma_1^2+\sigma_2^2\right)\right)}}\right)\right] \\ & +\frac{1/2}{\sqrt{2\pi}}\left(\frac{1}{\sigma_1}\exp\left(\frac{-\gamma^2}{2\sigma_1^2}\right)+\frac{1}{\sigma_2}\exp\left(\frac{-\gamma^2}{2\sigma_2^2}\right)\right)g(\gamma)+\frac{1}{4}\delta(\gamma). \end{aligned} \tag{13}$$

The optical power of HACO-OQAM-FBMC is given by

$$P_{\text{opt}} = \int_0^{\infty}\gamma f_{z_{\text{HACO-OQAM-FBMC}}}(\gamma)d\gamma. \tag{14}$$

The electrical power of HACO-OQAM-FBMC is given by

$$P_{\text{elc}} = \int_0^{\infty}\gamma^2 f_{z_{\text{HACO-OQAM-FBMC}}}(\gamma)d\gamma. \tag{15}$$

Equations (14) and (15) have no closed-form solution. Therefore, they are calculated using a numerical process.

The probability density function of HACO-OQAM-FBMC is given in Figure 4. It consists of both theoretical and simulated PDF and shows similar performance. The PDF curve shows that the proposed technique is power efficient.

3.2. Bit Error Probability (BEP) of HACO-OQAM-FBMC. The bit error probability of HACO-OQAM-FBMC is given by [23]

$$P_{\sqrt{M}} = 2\left(1-\frac{1}{\sqrt{M}}\right)Q\left(\sqrt{\frac{3}{M-1}\frac{S_{\text{av}}}{N_o}}\right), \tag{16}$$

where M is the constellation size and S_{av}/N_o is the average signal to noise ratio (SNR)/symbol.

Figure 5 shows the bit error rate (BER) performance of the HACO-OQAM-FBMC modulation technique. The FBMC overlapping factor ($k = 4$) is used for simulation. The theoretical and simulation results show almost similar performance.

As shown in Figure 6, the performance of HACO-OQAM-FBMC shows 2 dB degradation when compared with ACO-OFDM because only half of the power is allocated to odd subcarriers (ACO) in HACO-OQAM-FBMC. In reality, the performance of the proposed scheme is better when compared with ACO-OFDM because the OFDM performance is degraded due to the use of cyclic prefix (CP) [24]. The BER performance of the proposed technique is better than that of DCO-OFDM and ADO-OFDM because no DC bias is used, and hence, it is power efficient.

Analysis of Figure 7 shows that there is a 3 dB penalty for HACO-OQAM-FBMC as compared to ACO-FBMC, but actually both have similar performance because half power

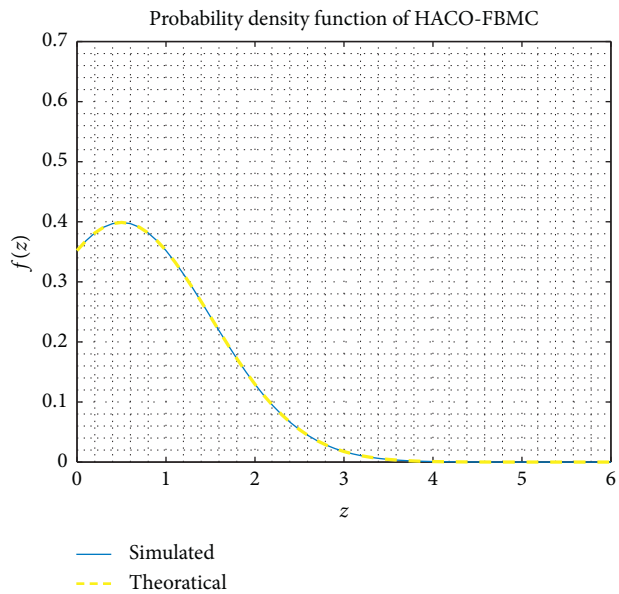

Figure 4: Probability density function of HACO-OQAM-FBMC.

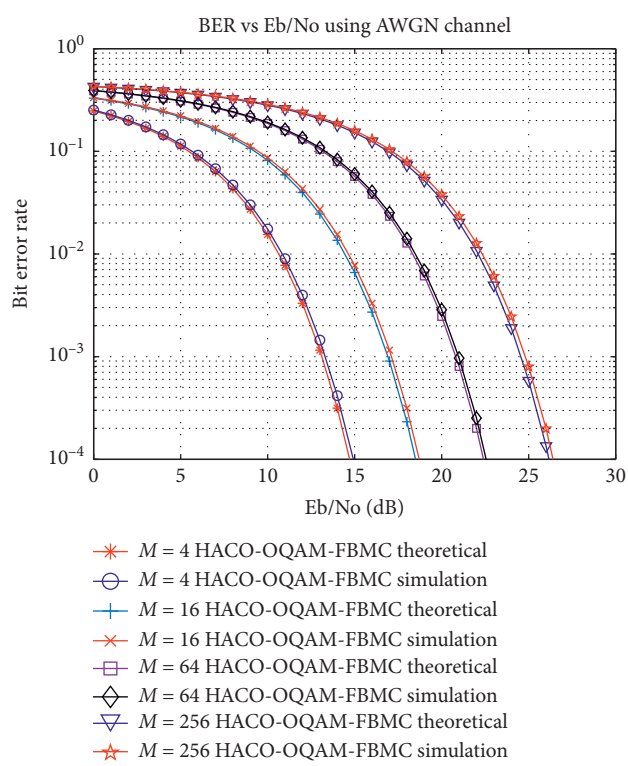

Figure 5: BER of HACO-OQAM-FBMC using 4-OQAM, 16-OQAM, 64-OQAM, and 256-OQAM modulation.

of HACO-OQAM-FBMC is contained by even subcarriers (PAM-DMT). The BER performance of the proposed technique is power efficient as compared to that of DCO-FBMC and EHACO-OFDM because no DC bias is used in the proposed technique.

3.3. Peak to Average Power Ratio (PAPR) of HACO-OQAM-FBMC. The PAPR of HACO-OQAM-FBMC is given by

$$\mathrm{PAPR}_{\mathrm{HADO}} = 10\log_{10}\left(\frac{\max[z]^2}{E\{[z]^2\}}\right). \tag{17}$$

The PAPR of ACO-OFDM, ACO-FBMC, DCO-OFDM, EHACO-OFDM, ADO-OFDM, DCO-OFDM, and HACO-OQAM-FBMC is given in Figure 8. ACO-OFDM has the best PAPR as compared to other techniques. The proposed method HACO-OQAM-FBMC PAPR can be reduced using

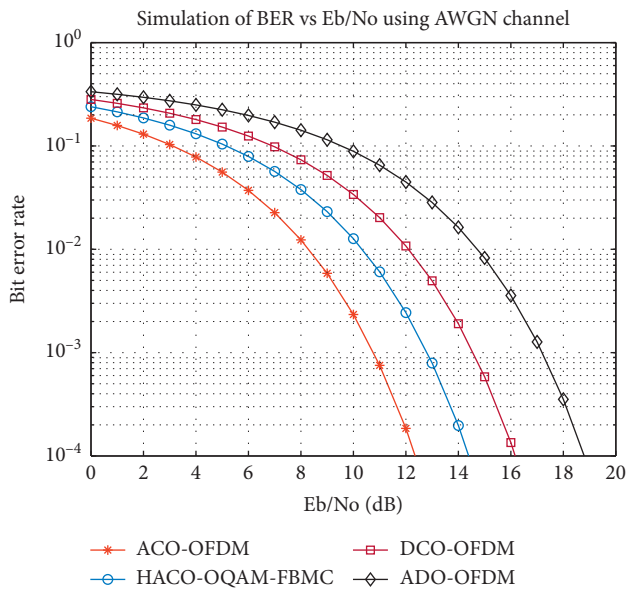

Figure 6: Simulation of BER of ACO-OFDM, DCO-OFDM, ADO-OFDM, and HACO-OQAM-FBMC.

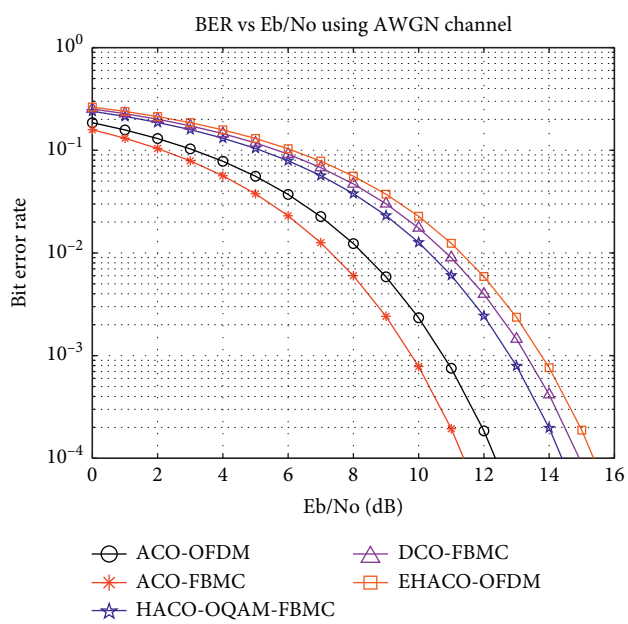

Figure 7: Simulation of BER of ACO-FBMC, DCO-FBMC, EHACO-OFDM, and HACO-OQAM-FBMC.

optimization algorithms. DCO-FBMC has the worst PAPR as compared to other techniques because of DC bias and the FBMC modulation technique.

3.4. Computational Complexity of HACO-OQAM-FBMC. The computational complexity of HACO-OQAM-FBMC is given by

$$\mathrm{RM}_{\mathrm{HF}} = M \times \left(4 \times \left(N \log_2 N - 3N + 4\right) + 8\mathrm{NK}\right), \quad (18)$$

where $\mathrm{RM}_{\mathrm{HF}}$ is the number of real multiplications for HACO-OQAM-FBMC. M is the constellation size, N is the number of subcarriers, and K is the overlapping factor.

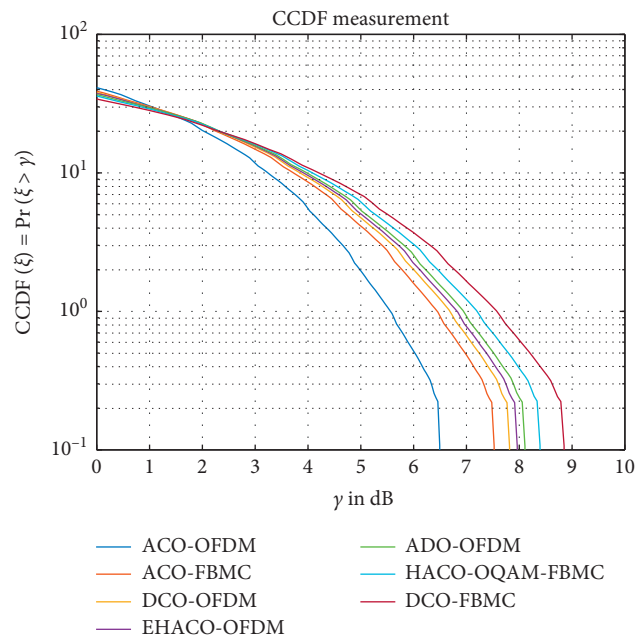

Figure 8: Simulation of peak to average power ratio (PAPR) of ACO-OFDM, ACO-FBMC, DCO-OFDM, EHACO-OFDM, ADO-OFDM, DCO-OFDM, and HACO-OQAM-FBMC.

$$\mathrm{RA}_{\mathrm{HF}} = M \times \left(4 \times \left(N \log_2 N - 3N + 4\right) + 8\mathrm{NK}\right), \quad (19)$$

where $\mathrm{RA}_{\mathrm{HF}}$ is the number of real additions for HACO-OQAM-FBMC.

The computational complexity of HACO-OQAM-FBMC is given in Figures 9 and 10. The computational complexity of ACO-OFDM is the lowest as compared to other techniques because of the no-DC bias technique and use of OFDM. OFDM has low computational complexity than FBMC [25]. HACO-OQAM-FBMC technique computational complexity is the highest among other techniques because extra processing is required for PAM-DMT signals.

3.5. Spectral Efficiency (SE) of HACO-OQAM-FBMC. The spectral efficiency of HACO-OQAM-FBMC can be calculated from [4]

$$\eta = \alpha\zeta\left(1 - P_{\sqrt{M}}\right)\nu_T\nu_F, \quad (20)$$

where α is the coding rate of channel, ζ = Number of bits/Subcarrier = $\log_2(M)$, and $\nu_T\nu_F$ is the time-frequency efficiency.

The spectral efficiency of ACO-OFDM, DCO-OFDM, ACO-FBMC, DCO-FBMC, EHACO-OFDM, and HACO-OQAM-FBMC is given in Figure 11. The spectral efficiency of HACO-OQAM-FBMC is higher than that of other modulation techniques and almost similar to that of DCO-FBMC because DCO-FBMC does not use Hermitian symmetry and, hence, has more subcarriers for data communication. All other modulation techniques have low spectral efficiency as compared to the proposed method because they are OFDM-based techniques which have low spectral efficiency as compared to FBMC [25].

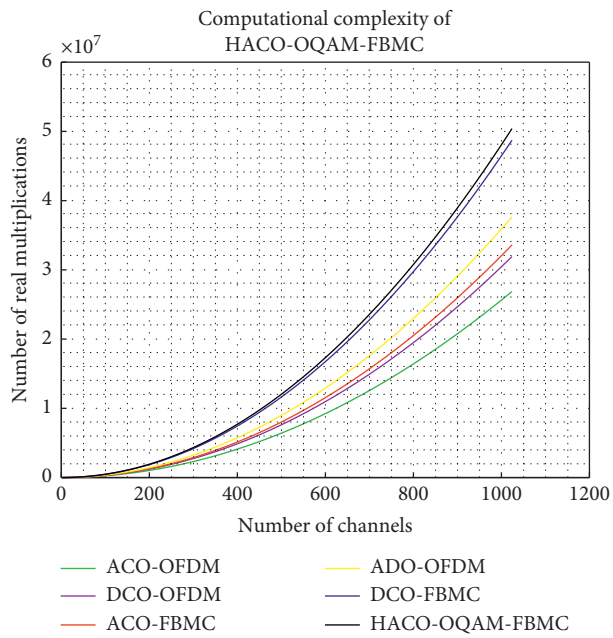

Figure 9: Simulation of computational complexity (multiplications) of ACO-OFDM, ACO-FBMC, DCO-OFDM, ADO-OFDM, DCO-OFDM, and HACO-OQAM-FBMC.

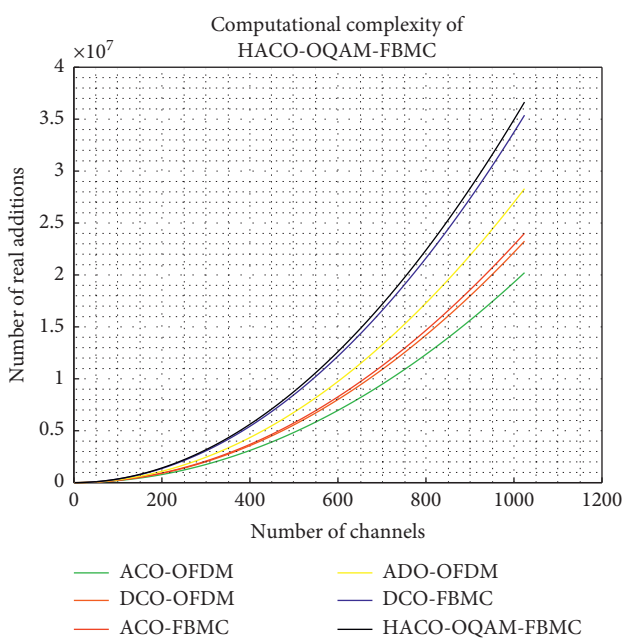

Figure 10: Simulation of computational complexity (additions) of ACO-OFDM, ACO-FBMC, DCO-OFDM, ADO-OFDM, DCO-OFDM, and HACO-OQAM-FBMC.

3.6. Power Spectral Density (PSD) of HACO-OQAM-FBMC. The power spectral density of HACO-OQAM-FBMC is shown in Figure 12. PSD of ACO-FBMC, DCO-FBMC, and HACO-OQAM-FBMC is the same because the same prototype filter is used. The PSD of the proposed technique is better than that of the OFDM-based technique because FBMC has low out-of-band distortion as compared to OFDM.

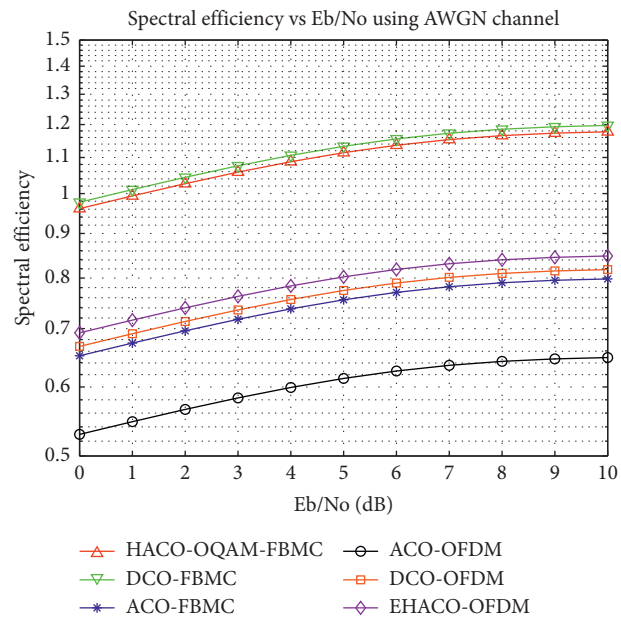

Figure 11: Spectral efficiency of HACO-OQAM-FBMC, ACO-OFDM, DCO-OFDM, EHACO-OFDM, DCO-FBMC, and ACO-FBMC.

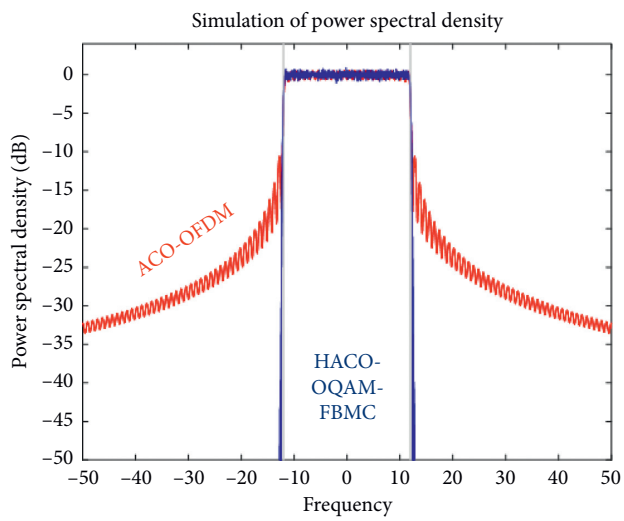

Figure 12: Simulation of the power spectral density (PSD) of ACO-OFDM and HACO-OQAM-FBMC.

4. Conclusions

This research work proposes Hybrid FBMC schemes for visible light communication based on an intensity modulation/direct detection (IM/DD) channel. In hybrid asymmetrically clipped DC biased optical FBMC (HACO-OQAM-FBMC), ACO-FBMC is used for the odd subcarriers and for even subcarriers, PAM-DMT is used. The PAPR of the proposed scheme is 0.96 dB more than ACO-FBMC because of hybridization. The spectral efficiency of HACO-OQAM-FBMC is higher than that of ACO-OFDM, DCO-OFDM, ACO-FBMC, and EHACO-OFDM due to use of even subcarriers and the FBMC multicarrier modulation

technique. The computational complexity of HACO-OQAM-FBMC is higher because extra processing is required for even subcarriers. It is shown that there is no interference on odd subcarriers because PAM-DMT and receiver demodulation is achieved using the clipping estimation technique. Future directions can be reducing computational complexity and PAPR of HACO-OQAM-FBMC.

Data Availability

The data used to support the findings of this study in the manuscript are available from the corresponding author upon request.

Conflicts of Interest

The authors declare that they have no conflicts of interest.

Acknowledgments

The authors gratefully acknowledge the support of Council of Scientific and Industrial Research (CSIR), New Delhi, under the Senior Research Fellowship grant 09/135/(0798)/18-EMR-I.

References

[1] R. Nissel, S. Schwarz, and M. Rupp, "Filter bank multicarrier modulation schemes for future mobile communications," *IEEE Journal on Selected Areas in Communications*, vol. 35, no. 8, pp. 1768–1782, 2017.

[2] S. Kumar and P. Singh, "A comprehensive survey of visible light communication: potential and challenges," *Wireless Personal Communications*, vol. 109, no. 2, pp. 1357–1375, 2019.

[3] X. Zhang, C. Zhang, M. Zhu et al., "SSB pruned DFT-spread FBMC signal with low PAPR in direct-detection PONs," *IEEE Photonics Journal*, vol. 12, no. 3, 2020.

[4] Y. Liu, X. Chen, Z. Zhong et al., "Waveform design for 5G networks: analysis and comparison," *IEEE Access*, vol. 5, pp. 19282–19292, 2017.

[5] S. Kumar and P. Singh, "Filter bank multicarrier modulation schemes for visible light communication," *Wireless Personal Communications*, vol. 113, no. 4, pp. 2709–2722, 2020.

[6] T. C. Bui, S. Kiravittaya, K. Sripimanwat et al., "A comprehensive lighting configuration for efficient indoor visible light communication networks," *International Journal of Optics*, vol. 14, 2016.

[7] M. A. Al-Jarrah, A. Al-Dweik, K.-H. Park, and M.-S. Alouini, "Amplitude-coherent detection for optical wireless communications: opportunities and limitations," *IEEE Open Journal of the Communications Society*, vol. 1, pp. 550–562, 2020.

[8] J.-Y. Wang, C. Liu, J.-B. Wang, Y. Wu, M. Lin, and J. Cheng, "Physical-layer security for indoor visible light communications: secrecy capacity analysis," *IEEE Transactions on Communications*, vol. 66, no. 12, pp. 6423–6436, 2018.

[9] J. Y. Wang, Q. L. Li, J. X. Zhu, and Y. Wang, "Impact of receiver's tilted angle on channel capacity in VLCs," *Electronics Letters*, vol. 53, no. 6, pp. 421–423, 2017.

[10] J. Armstrong and B. Schmidt, "Comparison of asymmetrically clipped optical OFDM and DC-biased optical OFDM in AWGN," *IEEE Communications Letters*, vol. 12, no. 5, pp. 343–345, 2008.

[11] X. Zhang, Y. F. Zhou, Y. P. Yu et al., "Comparison and analysis of DCO-OFDM, ACO-OFDM and ADO-OFDM in IM/DD systems," *Applied Mechanics and Materials*, vol. 701, pp. 1059–1062, 2015.

[12] R. Guan, N. Huang, J. Y. Wang et al., "Enhanced hybrid asymmetrically clipped orthogonal frequency division multiplexing for optical wireless communications," *Optical Engineering*, vol. 55, no. 5, 2016.

[13] S. Dimitrov, S. Sinanovic, and H. Haas, "Signal shaping and modulation for optical wireless communication," *Journal of Lightwave Technology*, vol. 30, no. 9, pp. 1319–1328, 2012.

[14] M. G. Bellanger, "Specification and design of a prototype filter for filter bank based multicarrier transmission," *IEEE*, vol. 4, pp. 2417–2420, 2001.

[15] S. Mirabbasi and K. Martin, "Design of prototype filter for near-perfect-reconstruction overlapped complex-modulated transmultiplexers," *IEEE*, vol. 1, 2002.

[16] J. Yang and Y. Chen, "Indoor localization using improved rss-based lateration methods," *IEEE*, vol. 1, 2009.

[17] J. Armstrong and A. J. Lowery, "Power efficient optical OFDM," *Electronics Letters*, vol. 42, no. 6, pp. 370–372, 2006.

[18] L. Chen, B. Krongold, and J. Evans, "Performance analysis for optical OFDM transmission in short-range IM/DD systems," *Journal of Lightwave Technology*, vol. 30, no. 7, pp. 974–983, 2012.

[19] D. J. Barros, S. K. Wilson, and J. M. Khan, "Comparison of orthogonal frequency-division multiplexing and pulse-amplitude modulation in indoor optical wireless links," *IEEE Transactions on Communications*, vol. 60, no. 1, pp. 153–163, 2011.

[20] X. Li, R. Mardling, and J. Armstrong, "Channel capacity of IM/DD optical communication systems and of ACO-OFDM," *IEEE*, vol. 60, pp. 2128–2133, 2007.

[21] I. S. Gradshteyn and I. M. Ryzhik, "Table of integrals, series, and products," 2000.

[22] B. Ranjha and M. Kavehrad, "Hybrid asymmetrically clipped OFDM-based IM/DD optical wireless system," *Journal of Optical Communications and Networking*, vol. 6, no. 4, pp. 387–396, 2014.

[23] J. G. Proakis and M. Salehi, "Digital communications," 2014.

[24] B. Muquet, Z. Zhengdao Wang, G. B. Giannakis et al., "Cyclic prefixing or zero padding for wireless multicarrier transmissions?," *IEEE Transactions on Communications*, vol. 50, no. 12, pp. 2136–2148, 2002.

[25] B. de Courville, "OFDM versus filter bank multicarrier," *IEEE Signal Processing Magazine*, vol. 28, no. 3, pp. 92–112, 2011.